

**ENVIRONMENTAL EFFECTS AND CURE MONITORING OF
MULTIFUNCTIONAL COMPOSITES OF CARBON NANOTUBES**

by

Kalon L. Lasater

A thesis submitted to the Faculty of the University of Delaware in partial fulfillment of the requirements for the degree of Master of Science in Mechanical Engineering

Summer 2012

© 2012 Kalon L. Lasater
All Rights Reserved

**ENVIRONMENTAL EFFECTS AND CURE MONITORING OF
MULTIFUNCTIONAL COMPOSITES OF CARBON NANOTUBES**

by

Kalon L. Lasater

Approved: _____
Erik. T. Thostenson, Ph.D.
Professor in charge of thesis on behalf of the Advisory Committee

Approved: _____
Suresh G. Advani, Ph.D.
Chair of the Department of Mechanical Engineering

Approved: _____
Babatunde A. Ogunnaike, Ph.D.
Interim Dean of the College of Engineering

Approved: _____
Charles G. Riordan, Ph.D.
Vice Provost for Graduate and Professional Education

ACKNOWLEDGMENTS

Erik T. Thostenson, Ph.D. is thanked for his advisement, support and creativity. Norbert Mulders, Ph.D. and Jonghwan Suhr, Ph.D. are acknowledged for serving on the thesis defense committee headed by Erik T. Thostenson. Aaron Ram, B.S. of Vishay Precision Resistors is thanked for data acquisition support. Steve Sauerbrunn, Ph.D. of Mettler Toledo provided training and input on the thermomechanical analyzer. The work on the environmental testing of fiber composites was inspired by the studies of the late Thomas S. Gates, Ph.D. of the NASA Langley Research Center. A special appreciation is extended to Saeed Ziaee, Ph.D. and Beckry Abdel-Magid, Ph.D. of the Department of Composite Materials Engineering at Winona State University, Winona, Minnesota. Beckry Abdel-Magid supplied the weathering fixture used in environmental testing. Saeed Ziaee provided useful perspective into polymer morphology and thermal analysis. The help and guidance of post-doctoral researcher Amanda S. Wu, Ph.D. is acknowledged. Joe Deitzel, Ph.D. of the Center for Composite Materials provided training on the rheometer. This research was funded by the Air Force Research Laboratory (AFRL) Award No. FA9559-11-C-0003 (Phase II STTR with Acellent Technologies, Dr. David Stargel, Program Manager). The cure monitoring work was made possible by the National Science Foundation (NSF) and the National Research Foundation of Korea (NRF) under the 2011 East-Asia and Pacific Summer Institutes (EAPSI) Fellowship, NSF award ID no. 1108043. The author was hosted at Seoul National University, Seoul, Korea with the laboratory of Woong-Ryeol Yu, Ph.D. and at the

Korea Institute of Materials Science (KIMS) in Changwon, Korea under Byung-Sun Kim, Ph.D. A very special appreciation is extended to graduate students Wonjin Na, B.S. and Seokjin Hong, M.S. of the Smart Composite Materials Research Laboratory at Seoul National University for their research assistance and sincere friendship.

TABLE OF CONTENTS

LIST OF TABLES	vii
LIST OF FIGURES	viii
ABSTRACT	xii

Chapter

1	INTRODUCTION	1
1.1	Motivation and Scope	1
1.2	Carbon Nanotubes: Mechanical and Electrical Properties	3
1.3	Carbon Nanotube / Polymer Nanocomposites: Property Enhancement and Processing Challenges	5
1.4	Carbon Nanotube-Reinforced Structural Composites: Multiscale and Multifunctional	7
1.5	Multifunctionality in Composites of Carbon Nanotubes.....	11
2	PROCESSING OF NANOCOMPOSITES	13
2.1	Synthesis of Vinyl Ester Resin	13
2.2	Dispersion of Carbon Nanotubes by Calendering	14
2.3	Dispersion by Functionalization and Ultrasonication of Carbon Nanotubes	16
2.4	Fabrication of Multifunctional Fiber-Reinforced Composites	17
3	EXPERIMENT DESIGN AND INSTRUMENTATION	20
3.1	Combined Thermomechanical / Thermoresistive Analysis	20
3.1.1	Background.....	20
3.1.2	<i>In Situ</i> Electrical Resistance Measurements and Thermomechanical Analysis	21
3.2	<i>In Situ</i> Measurements during Environmental Testing	25
3.2.1	Background.....	25
3.2.2	Instrumentation.....	26

3.3	<i>In Situ</i> Electrical Resistance Measurements during Torsional Braid Analysis	29
3.3.1	Background.....	29
3.3.2	Instrumentation.....	30
4	THERMORESISTIVE CHARACTERIZATION OF CARBON NANOTUBE/VINYL ESTER COMPOSITES	34
4.1	Results and Discussion	34
4.1.1	Thermoresistive Response under Thermal Cycling	34
4.1.2	Thermomechanical / Thermoresistive Analysis	39
4.1.3	Summary.....	46
5	COMBINED THERMAL AND MECHANICAL LOADING OF COMPOSITES OF GLASS FIBER/CARBON NANOTUBE/VINYL ESTER.....	48
5.1	Results and Discussion	48
5.1.1	Pre-Tensioning of Composite Specimens	48
5.1.2	Sensing of Stress Relaxation and Damage during Environmental Testing	50
5.1.3	Summary.....	56
6	<i>IN SITU</i> CURE MONITORING OF GLASS FIBER/CARBON NANOTUBE/VINYL ESTER COMPOSITES	58
6.1	Results and Discussion	58
6.1.1	Isothermal Cure of CNT/VE Composites.....	59
6.1.2	Electrical Resistance during Continuous Heating Cure	62
6.1.3	Viscoelastic Trends during Torsional Braid Analysis.....	63
6.1.4	Summary.....	65
7	CONCLUSIONS	67
	REFERENCES	70
Appendix		
A	REFERENCES FOR REPRODUCED FIGURES.....	76
B	AUTHOR'S PUBLICATIONS AND WORKS IN PROGRESS	77
C	BIOGRAPHY.....	78

LIST OF TABLES

Table 3.1:	Average electrical resistance range during thermal cycling and value of reference resistor used for each specimen group.	24
Table 4.1:	Comparison of the thermoresistive and thermomechanical methods for sensing T_g showing the average of three specimens.	42

LIST OF FIGURES

Figure 1.1: “Rolling” of graphene sheet to form a single-walled carbon nanotube. ...	5
Figure 1.2: Transmission electron microscopy image of a multi-walled carbon nanotube showing concentric nanotube morphology [16]. Produced with permission from IOP Publishing.	5
Figure 1.3: TEM micrograph of CNT/polystyrene composite film showing crack region with nanotube pullout and breakage [17]. Reprinted with permission from American Institute of Physics.	7
Figure 1.4: Multiscale architectures for composite materials; a) CNTs grown on silica fibers from CVD process [20]; b) CNTs dispersed in matrix [23]. Reproduced with permissions from Elsevier.	8
Figure 1.5: SEM micrographs of fracture surface of a multiscale composite showing individual nanotubes bridging the fiber/matrix interfacial region [22]. CNTs were deposited on the carbon fiber using an electrophoresis method. Reproduced with permission from American Chemical Society.	9
Figure 1.6: Electrical resistance (a) and acoustic emissions (b) response to quasi-static tensile loading and reloading of a cross-ply composite with CNTs dispersed in a vinyl ester matrix [25]. Reproduced with permission from Elsevier.	10
Figure 1.7: Illustration of tunneling-based sensing using carbon nanotubes dispersed in a polymer matrix.	12
Figure 2.1: Esterification reaction of EPON 862 with methacrylic acid to form vinyl ester monomer [31]. Reproduced with permission from Elsevier.	14
Figure 2.2: Schematic of 3-roll-mill showing key parameters of the high shear mixing process [31]. Reproduced with permission from Elsevier.	15
Figure 2.3: Diagram of apparatus used to oxidize and sonicate carbon nanotubes [32]. Reproduced with permission from Elsevier.	17

Figure 2.4:	Schematic showing vacuum assisted resin transfer molding processing technique used to fabric multifunctional composites [22]. Reproduced with permission from American Chemical Society.	18
Figure 2.5:	Photograph of glass fiber preform being infused with vinyl ester resin with dispersed CNTs. Used with permission of E.T. Thostenson.....	19
Figure 3.1:	Photograph of nanocomposite specimen mounted on the TMA stage for thermoresistive characterization.	23
Figure 3.2:	Electrical circuit and data acquisition interface diagram.	24
Figure 3.3:	Constant displacement weathering fixture used for environmental testing of composites.	27
Figure 3.4:	Typical temperature and humidity profiles during a thermal cycle.	28
Figure 3.5:	Temperature profiles used during torsional braid analysis.	31
Figure 3.6:	Image of a 0.25 wt% CNT/VE TBA specimen showing zoom in of electrode area.....	32
Figure 3.7:	Images of TBA set-up, left; AR-2000 rheometer with Environmental Testing Chamber (ETC) and torsion accessory attached, right; torsion clamp with 0.1 wt% CNT/VE specimen mounted.	32
Figure 4.1:	Normalized electrical resistance change of CNT/VE composites during iterative thermal cycling from 25 to 165 °C; dashed lines and numbering showing thermal cycle iteration.	35
Figure 4.2:	Normalized electrical resistance change versus temperature of CNT/VE composites during thermomechanical testing.....	37
Figure 4.3:	Normalized electrical resistance change during the isothermal segments at 165 °C showing diffusion-like increase in overall resistance (R_0 taken at initial 165 °C set-point).	38
Figure 4.4:	Electrical resistance change of CNT/VE composites during the final ramp-up segment; right: unfiltered data for 0.1 wt% specimen, left: local minima indicating T_g locations for specimens with greater than 0.1 wt% CNT (note that 0.5-0.75 wt% data are offset by 2 and 0.5 % resistance change, respectively, to clearly show the curves).	40

Figure 4.5:	TMA results for 1 wt% CNT/VE specimen showing dimensional changes during heating and the calculated linear thermal expansion curve showing the T_g location.	41
Figure 4.6:	Comparison of volume resistivity and dimensional change curves for CNT/VE composites during final ramp-up segment.	44
Figure 4.7:	TCR curves for composites of CNT and vinyl ester during final ramp-up segment showing difference in thermoresistive trends for 0.5-1 versus 0.1 wt% composites.	45
Figure 5.1:	Pre-tensioning step: typical time lapse showing electrical resistance and longitudinal and transverse strains.	49
Figure 5.2:	Normalized electrical resistance change of four specimens versus longitudinal strain during manual tensioning of specimens inside of weathering fixture.	49
Figure 5.3:	Typical electrical resistance trend during prolonged thermal cycling in an environmental chamber while constrained in a weathering fixture; dashed lines show maximum and minimum temperature contours and average 25 °C contour.	51
Figure 5.4:	Normalized electrical resistance change during the initial thermal cycling segments showing permanent reduction in resistance due to stress relaxation above T_g	51
Figure 5.5:	Normalized resistance change during the first two cooling ramps to -73 °C; left: first cooling ramp showing step-like damage events, right: second cooling ramp showing little to no additional damage.	53
Figure 5.6:	Micrographs of edge replicas showing crack growth and accumulation in 90 ° plies at different stages of testing; a) initial condition, b) pre-tensioned condition, and c) post-thermal cycled condition.	54
Figure 5.7:	Normalized electrical resistance change during the final thermal cycle; slope change around 100 °C attributed to increase in matrix CTE across the glass transition.	56
Figure 6.1:	Electrical resistance response of a cured CNT/VE TBA specimen to a 1 Hz torsional oscillation; resistance versus time, data points traced with a cubic spline fit.	58

Figure 6.2: Comparison of isothermal cure data for neat VE and CNT/VE TBA specimens at 30 °C; storage and loss moduli and electrical resistance (delta for neat VE) versus time.....	60
Figure 6.3: Delta and normalized electrical resistance change (filtered) for a 0.25 wt% CNT/VE specimen during isothermal cure at 30 °C; dashed lines separating gelation and vitrification regions.	61
Figure 6.4: Electrical resistance change and delta during continuous heating cure for 0.5 and 0.25 wt% CNT specimens; left: dashed lines separating gelation and vitrification region and the glass transition. Note that the material passes back into the rubbery phase after the glass transition at 142 °C.....	62
Figure 6.5: Electrical resistance change during post-cure of 0.25 and 0.5 wt% CNT/VE specimen after undergoing continuous heating cure; curves show diffusion-like increase in resistance.	63
Figure 6.6: Comparison of viscoelastic trends during ramping segments of continuous heating cured, left (Profile III), and isothermal cured specimens of 0.5 wt% CNT/VE, right (Profile I).....	64
Figure 6.7: Electrical resistance change (filtered) and shear moduli during TBA tests; 0.25 and 0.5 wt% CNT/VE specimens using Profiles II and I, respectively (refer to Figure 3.5).	65
Figure 7.1: Schematic showing the sensing of cure, post-cure and service life using the carbon nanotube-based sensing technology developed in this work.	67

ABSTRACT

In this work, composites of dispersed carbon nanotubes (CNTs) in a thermosetting polymer matrix were investigated. It was the goal of the study to develop *in situ* sensing technologies based on the measurement of electrical resistance of a percolating network of CNTs in the polymer matrix. Three characterization methods were developed and changes in state of the composites were correlated to changes in electrical resistance.

Composites of dispersed CNTs and vinyl ester (VE) resin were tested for thermoresistive behavior using a simple *in situ* electrical resistance measurement during thermomechanical analysis. Specimens ranging from 0.1 to 1 wt% CNT were tested. The results showed that the thermoresistive behavior was strongly dependent on the CNT content and was highly tailorable in terms of sensitivity to temperature and polymer segmental motion. Specimens with CNT concentrations far above the electrical percolation threshold showed positive and negative temperature coefficient of resistance (TCR) over the temperature range from 25 to 165 °C. Specimens with CNT concentration closer to the percolation threshold showed a near-zero and negative TCR. It was found that thermoresistive analysis of the CNT/VE composites was capable of detecting the glass transition and likely other polymer segmental and side chain processes previously observable only through more complex electrothermic analysis techniques.

Cross-ply composites of glass fiber and dispersed CNTs in VE resin were tested in an environmental chamber while constrained in a constant displacement weathering fixture. Temperature was repeatedly cycled at a high rate from -73 to 150 °C for approximately 56 hours. Electrical resistance was monitored in real-time during the duration of the testing regime, including the initial pre-tensioning step, and the evolution of damage observed in the electrical resistance data was assessed by edge replication. It was found that the electrical resistance response was sensitive to the combined thermal and mechanical loading condition and that significant cracking occurred in the 90 ° plies during environmental testing.

A novel method of *in situ* polymer matrix composite materials process monitoring was developed. The method of torsional braid analysis (TBA) was used in conjunction with a real-time data acquisition system to determine the viscoelastic behavior of VE/CNT/glass fiber composite test specimens. The data acquisition system was used to collect electrical resistance data from electrodes placed at either end of the specimen during TBA tests. A rheometer with torsion accessory served as an analog for the torsional pendulum. The sensitivity of nanotube-based sensing to viscoelastic changes during cure was investigated. It was observed that electrical resistance was strongly correlated to the progression of cure. The proposed sensing method has the potential to give real-time sensing capability during critical phases of manufacturing as well as in-service monitoring for enhanced safety and reliability.

Chapter 1

INTRODUCTION

1.1 Motivation and Scope

Starting after World War II, as composite materials replaced traditional materials in aerospace and marine applications, the study of long term performance and environmental effects had been of interest to many researchers [1-3]. It was generally found that property degradation in traditional fiber composites due to environmental effects was in matrix dominated properties, i.e. transverse, interlaminar and through thickness properties [4]. With the emergence of multifunctional materials and their expected use in aerospace and marine applications, the study of environmental effects on these new materials is of practical importance. To date, little research has been conducted on the effect of the environment on these promising materials. Understanding the effect of temperature, and thermal cycling on multifunctional materials is an important step towards their eventual use in industry. These materials have the potential to overcome many challenges facing polymer matrix composites for use in extreme environments [2], by providing *in situ* sensing and damage detecting functionality in addition to structural reinforcement.

Aerospace and marine applications are exposed to dramatic temperature and humidity fluctuations which, over time, can lead to poor performance and premature failure. Current methods of monitoring the health of critical structures often cannot be used during actual service, severely limiting their effectiveness in predicting failure. The Federal Aviation Administration's 2012 National Aviation Research Plan (2012

NARP) [5] includes *in situ* crack and damage detection as part of the National research agenda for the aviation industry. *In situ* sensing based on the electrical resistance measurements of a network of dispersed carbon nanotubes offers much potential in meeting this need of critical structures.

In addition to environmental effects, a considerable factor affecting the long-term performance of structural composite materials is the accumulation of residual stresses resulting from the manufacturing process and inherent anisotropy of fiber-reinforced composite materials. These stresses cause deformation and micro-scale damage in the structure which can affect its overall properties and performance and lead to premature failure [6]. Furthermore, the state of cure is difficult to accurately predict during manufacturing and there is a need to develop *in situ* process monitoring methods. With the trend in industry leading toward ever greater usage of composite materials to create structures of increasing size and complexity, there is a need to develop practical and scalable methods of monitoring composites manufacture processing, namely the cure and post-cure processes, in order to improve the quality, safety and reliability of composite materials. There is potential for advanced composites to include process monitoring functionality.

In this work, the question of how temperature and thermal cycling affect multifunctional composites of CNTs and vinyl ester (VE) resin was addressed. In the process, new and original experimental techniques were engineered and developed and significant phenomena were observed and investigated. The resulting data shed significant light on the sensing mechanisms involved and demonstrate the wide variety of functionalities this new class of materials can possess. Chapter 1 reviews the current research literature related to this thesis. In Chapter 2, the methods used for

synthesis and processing of nanocomposites are described in technical detail. Chapter 3 describes the instrumentation and experimental approaches taken to measure electrical resistance *in situ* under various testing conditions. Chapters 4 through 6 present the research results and discussion. Chapter 7 summarizes the important findings and discusses their significance and includes recommendations for future work. It is the goal of this work to extend the sensing capability of dispersed carbon nanotubes from damage sensing in the finished product, to temperature and environmental sensing, and to sensing during processing phases using the same basic measurement approach. By measuring the electrical resistance changes of the nanotube network during the manufacturing process and throughout its service life, useful information about the state of cure, residual stress development, thermomechanical properties, and damage accumulation may be obtained.

1.2 Carbon Nanotubes: Mechanical and Electrical Properties

Carbon nanotubes have some unique properties which make them suitable reinforcements in composite materials. Carbon nanotubes have diameters in the range of 5 – 200 nm and lengths up to thousands of μm , extreme axial stiffness ($> 1 \text{ TPa}$) and high strength (2-28.5 GPa) [7]. Their high aspect ratio (length/diameter) results in a large specific surface area with high Van der Waals interaction forces. This makes them easier to handle because nanotubes tend to cling to themselves instead of dispersing into air. Although this eases weighing operations and may alleviate some health concerns, the high surface area creates significant challenges in achieving a high level of dispersion in composites.

In addition to their unique mechanical properties, CNTs have some special chemical, thermal and electrical properties which have made them an object of intense study in many engineering, physics and chemistry disciplines. These properties are dependent on how they were synthesized. Some of the first methods used to produce CNTs were the arc-discharge and laser ablation methods which produced only small quantities at a time and contained a wider variety of carbon fullerenes [8,9]. The synthesis method most often used today is the Chemical Vapor Deposition (CVD) method because of its relative low cost and industrial scalability. CVD as a continuous process involves the metering of a hydrocarbon gas and a catalyst, which may be delivered as a gas or placed on the growth substrate, into a high-temperature environment ($> 600\text{ }^{\circ}\text{C}$). By controlling the processing parameters (time, temperature, flow rate, etc.) it is possible to selectively grow many forms of carbon nanotubes including single and multi-walled varieties.

A useful way to visualize the synthesis of CNTs is as the “rolling” of a graphene sheet or single layer of graphite (see Figure 1.1). When “rolled,” the hexagonal bonding lattice creates a chirality in the nanotube. This chirality dictates the whether the nanotube will have metallic or semiconductor-like electrical properties. Unfortunately, this aspect of CNTs cannot be controlled at this point. For multi-walled carbon nanotubes, which are concentric layers of nanotubes, this results is a random mixture of metallic and semiconductor properties [10-12]. A transmission electron microscopy (TEM) image of a multi-walled nanotube is shown in Figure 1.2. This fact aside, CNTs have been exploited for use in nanotube-based electronics and sensors [13,14,15].

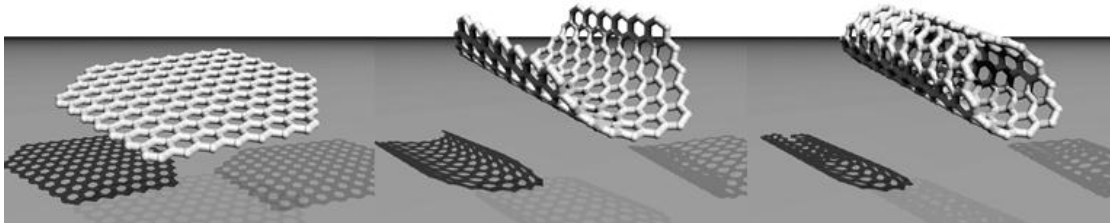


Figure 1.1: “Rolling” of graphene sheet to form a single-walled carbon nanotube.

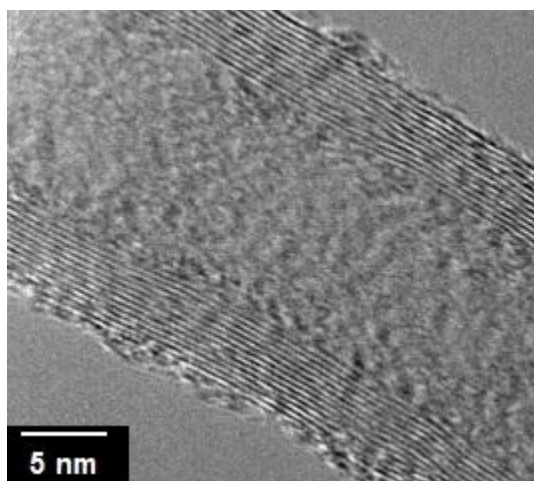


Figure 1.2: Transmission electron microscopy image of a multi-walled carbon nanotube showing concentric nanotube morphology [16]. Produced with permission from IOP Publishing.

1.3 Carbon Nanotube / Polymer Nanocomposites: Property Enhancement and Processing Challenges

In the last decade there has been a large focus on the research and development of nanoparticle reinforced polymers, with carbon nanotubes receiving most of the attention due to their high aspect ratio and extreme axial stiffness and strength. Qian and co-workers used a [17] solvent method to produce CNT/polystyrene films with random CNT alignment. The elastic modulus of the material was roughly 10 % less

than that predicted by a randomly orientated short-fiber composite approximation. Thostenson and Chou [16] used an aligned short-fiber elasticity model based on a distribution of nanotube length, diameter and alignment in polystyrene to accurately predict the experimental results for highly-aligned / highly dispersed nanocomposites. The drawn polystyrene saw an improvement in elastic modulus of nearly 90 % over neat polystyrene at 10 wt% CNT content. Gojny et al. [18] compared carbon black, single-walled, double-walled and multi-walled nanotubes, with and without amino-functionalization, dispersed in an epoxy matrix using a calendaring approach. They observed that the surface-functionalized nanotubes resulted in more significant improvements in elastic modulus (14 %), tensile strength (8 %) and especially fracture toughness (43 %). However, the improvements in fracture toughness were comparable to composites of carbon black.

A review by Thostenson et al. [7] summarizes much of the early efforts made to take advantage of CNTs as reinforcement in polymers, ceramics and metals. It was found that the CNT/polymer interfacial interactions were generally poor, leading to pull-out behavior or slipping during mechanical loading of the composites. This significantly limits their efficiency as reinforcement. A TEM image of a nanotube/polystyrene nanocomposite is shown in Figure 1.3. Obvious nanotube pull-out is evident, indicating that the nanotube/polymer adhesion is poor. Another significant hindrance to reinforcement was the dispersion of nanotubes in the matrix. The particular challenge of dispersion remains an important research topic. Many methods have been explored using CNT surface functionalization, ultrasonication, calendaring, *in situ* polymerization and surfactants, or combinations of these.

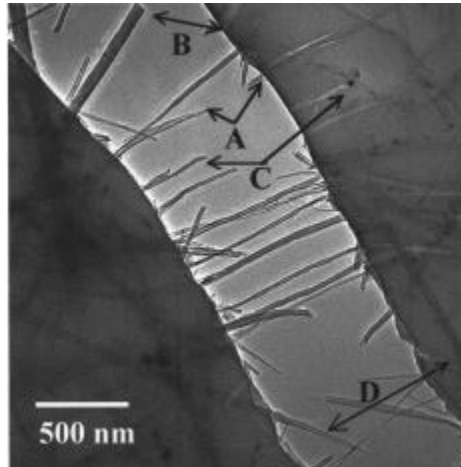


Figure 1.3: TEM micrograph of CNT/polystyrene composite film showing crack region with nanotube pullout and breakage [17]. Reprinted with permission from American Institute of Physics.

1.4 Carbon Nanotube-Reinforced Structural Composites: Multiscale and Multifunctional

Composite materials incorporating traditional continuous fiber reinforcement and matrix with dispersed carbon nanotubes were a natural progression from the nanotube/polymer nanocomposites discussed in Section 1.3. It was also discovered that the CVD process could be used to grow CNTs on the surface of carbon and glass fiber fabrics [19,20], forgoing the need for dispersion in the matrix. An alternative approach is to use electrophoretic deposition of CNTs in solution onto the fiber surfaces. Infusion of resin into the fabric results in a unique reinforcement architectures with nanotubes radiating from the fiber surfaces and bridging the gaps between individual fibers. Illustrations of two reinforcement architectures are shown in Figure 1.4. A review by Qian et al. [21] compared some of the processing methods and mechanical properties of “hierarchical” composites. It was generally found that the addition of CNTs improved the matrix-dominated properties, namely interlaminar

shear strength and fracture toughness. Figure 1.5 shows the mechanism behind the property enhancement: bridging of the fiber/matrix interphase [22].

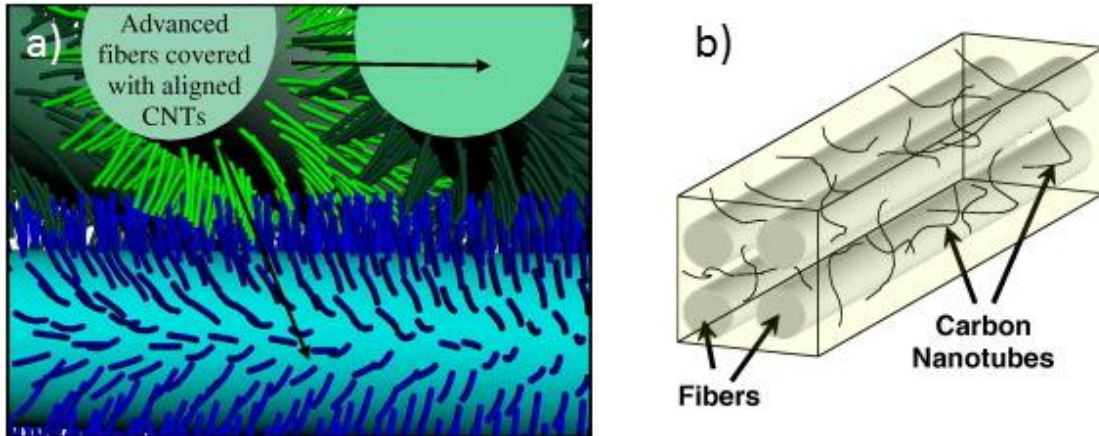


Figure 1.4: Mutliscale architectures for composite materials; a) CNTs grown on silica fibers from CVD process [20]; b) CNTs dispersed in matrix [23]. Reproduced with permissions from Elsevier.

Besides modifying the matrix dominated properties of fiber-reinforced composites, the addition of CNTs in the matrix phase can result in an electrically conducting network of nanotubes. Electrical percolation can be achieved at ultra-low CNT concentrations, often below 0.1 wt%. This resulted in the discovery of several sensing phenomena based on the electrical properties of carbon nanotube composites, which have, arguably, the greatest significance to the field of composite materials engineering and are the subjects of this thesis. Thostenson and Chou [24] developed approaches for sensing of deformation and microcracks using a percolating network of CNTs the polymer matrix of a fiber reinforced composite. Sensing was realized by measuring the direct current (DC) electrical resistance of the composite during various

loading regimes. The unique ability to form networks has enabled their use as materials where piezoresistivity, the change of resistivity/conductivity with applied deformation that is higher than expected based on simple dimensional change, can be exploited in a variety of applications. A combination of linear and non-linear piezoresistive behavior was observed, with the non-linearity resulting from material damage, i.e. matrix cracking. Figure 1.5 shows individual CNTs bridging a micron-sized crack in a multiscale composite and indicates the need for nano-scale sensors for detecting micro-scale damage.

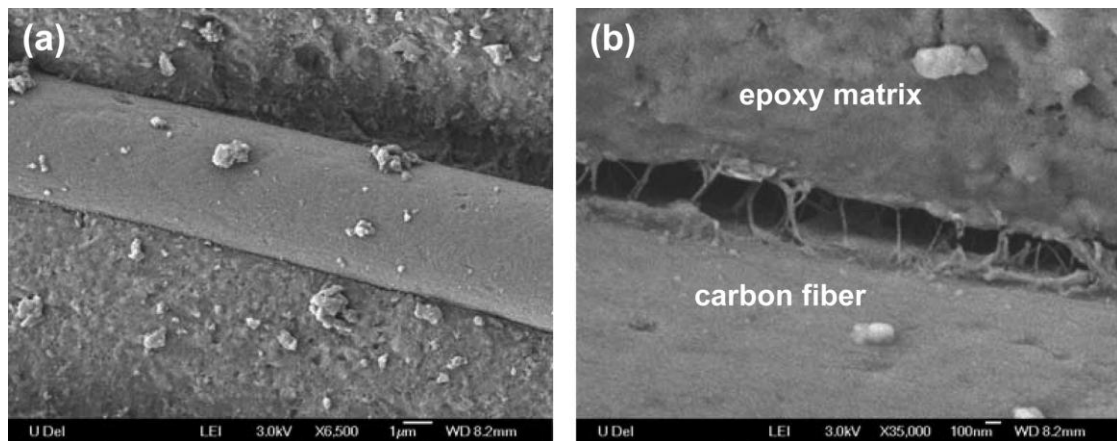


Figure 1.5: SEM micrographs of fracture surface of a multiscale composite showing individual nanotubes bridging the fiber/matrix interfacial region [22]. CNTs were deposited on the carbon fiber using an electrophoresis method. Reproduced with permission from American Chemical Society.

In a work by Gao et al. [25] the electrical resistance, stress, strain and acoustic emissions (AE) were monitored simultaneously during tensile loading of multifunctional cross-ply composites of glass fiber and vinyl ester resin with dispersed CNTs. The typical electrical resistance / AE / strain response of a cross-ply glass fiber

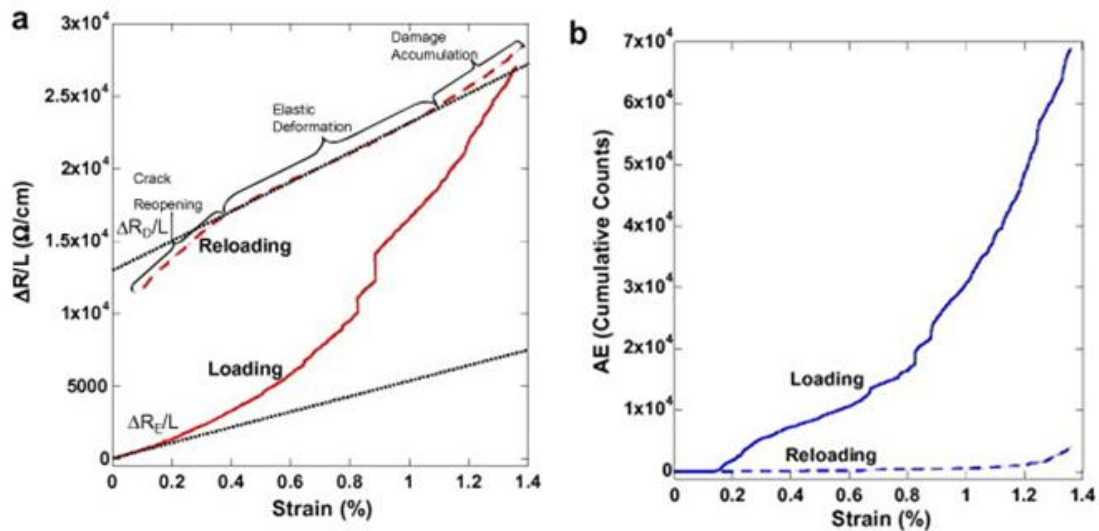


Figure 1.6: Electrical resistance (a) and acoustic emissions (b) response to quasi-static tensile loading and reloading of a cross-ply composite with CNTs dispersed in a vinyl ester matrix [25]. Reproduced with permission from Elsevier.

composite with CNTs dispersed in the matrix is shown in Figure 1.6. The real-time measurement of AE and electrical resistance during tensile loading and reloading shows a linear piezoresistive response during the first part of the initial loading (up to about 0.2 % strain). During this elastic deformation region, no acoustic emission events are recorded. After damage initiation at 0.2 % strain (typical initial damage strain value for cross-ply composites) additional damage accumulation is evidenced by the AE data and the electrical resistance increases in a similar manner. The damage events are typically caused by matrix cracking, fiber fracture and fiber/matrix debonding, all of which can be detected using AE. After unloading, reloading of the specimen revealed little additional AE but a permanent change in initial electrical resistance with distinctive crack reopening and elastic deformation regions were observed. The result showed that damage detection using CNTs was extremely

sensitive to the tensile loading regime. Thostenson and co-workers have gone on to demonstrate the ability to sense micro-scale damage under quasi-static, impact and cyclic loading conditions in glass fiber reinforced composites and bonded joints [26-29].

1.5 Multifunctionality in Composites of Carbon Nanotubes

The piezoresistivity and damage sensing functionality observed in previous works is thought to have its origin in the changes occurring in the CNT/CNT interphase, or tunneling gap [30]. At electrical percolation, when a sufficient amount of carbon nanotubes are dispersed in a polymer matrix are in electrical contact, the polymer layer between individual nanotubes is thin enough to allow sufficient transfer of electrons for electrical conductivity in the bulk material. When the material stretched the average tunneling gap increases and, therefore, the resistance to conduction increases. This explains the piezoresistive response described previously. The response to matrix cracking may be understood by considering the material as a network of resistors in parallel; by cutting a resistor off, the equivalent resistance will be greater.

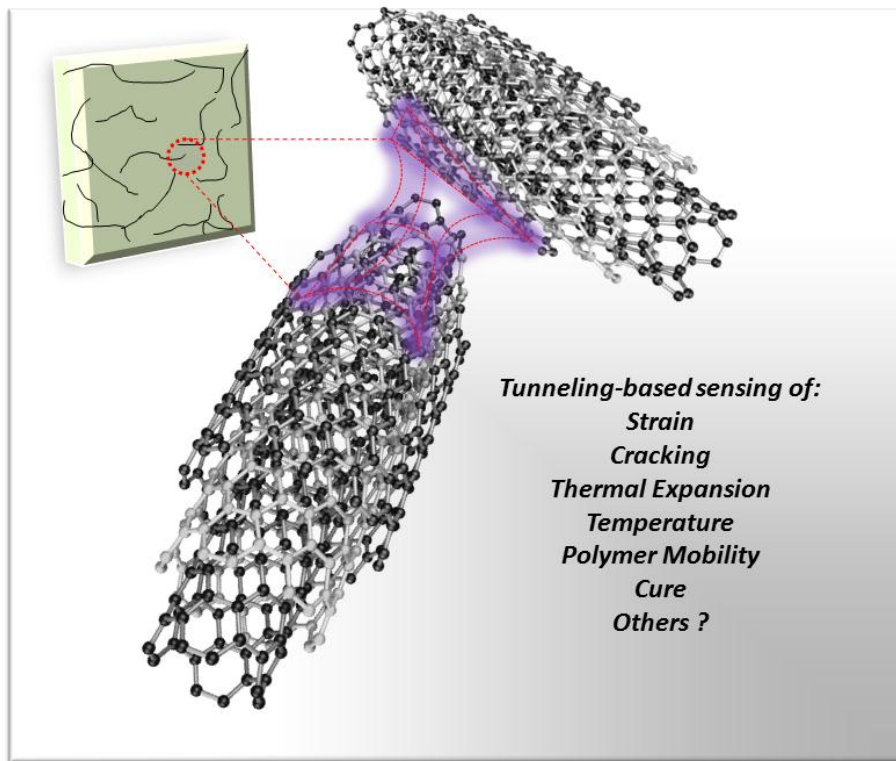


Figure 1.7: Illustration of tunneling-based sensing using carbon nanotubes dispersed in a polymer matrix.

Because of the tunneling effect, the bulk resistivity also increases with increasing dielectric constant of the polymer matrix. It should then be expected that tunneling-based sensing can detect a wider variety of changes taking place in the tunneling region: the polymer. This concept is illustrated in Figure 1.7. It will be shown in this thesis that the sensing method employed by Thostenson and co-workers is capable of detecting temperature, thermal expansion, polymer mobility and cure in addition to deformation and cracking. These observations are discussed in detail in Chapters 4 through 6.

Chapter 2

PROCESSING OF NANOCOMPOSITES

2.1 Synthesis of Vinyl Ester Resin

Vinyl ester resins are commonly used in industry because of their low viscosity and tailorable curing characteristics which make them suitable for many out-of-autoclave resin infusion processes. Commercial vinyl ester (VE) resins are available as blends of VE monomer and styrene monomer. This limits their processability in certain mixing operations because of the high volatility of the styrene component. For this reason, the VE resins used in this work were synthesized in-house from commercially available precursor materials such as epoxy and styrene monomers using previously established procedures [31].

VE monomer was synthesized from a bisphenol-F type epoxy monomer (EPON Resin 862, Momentive, USA) and methacrylic acid with triphenylphosphine and triphenylantimony (III) (99 %, Sigma-Aldrich, USA) as catalysts at 0.25 and 0.75 wt%, respectively. A batch of 100 g epoxy was reacted at 90 to 95 °C while stirring for 2 hr and allowed to cool to room temperature. As shown in Figure 2.1, the esterification reaction involves the opening of the epoxy ring groups and subsequent termination with the ester groups forming VE monomer. Fourier transform infrared spectroscopy (FTIR) was used in the development of this synthesis method to track the conversion of epoxy groups and to determine the proper reaction time and temperature for complete epoxy conversion [31]. Styrene monomer (≥ 99 %, ReagentPlus, Sigma-Aldrich, USA) was mixed at a later stage with the vinyl ester monomer at 40 wt%.

Immediately prior to vacuum infusion or other processing methods, the accelerator (6 % cobalt naphthenate in mineral spirits, Sigma-Aldrich, USA) and curing agent (Trigonox 239, AzkoNobel, USA) were added at 0.2 and 1 wt%, respectively. Trigonox 239 is a commercially available blend of peroxides.

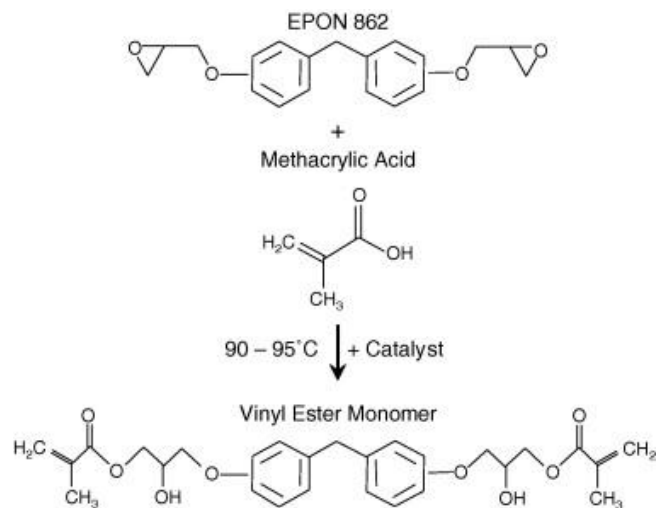


Figure 2.1: Esterification reaction of EPON 862 with methacrylic acid to form vinyl ester monomer [31]. Reproduced with permission from Elsevier.

2.2 Dispersion of Carbon Nanotubes by Calendering

Calendering methods require the use of stable non-volatile mixing media because of the high surface area to mixing-volume ratio involved. For this reason, CNTs (CM-95, Hanwha Nanotech, Korea) were dispersed in VE monomer and not the VE/styrene blends available commercially. The nanotubes were produced by thermal CVD and have a multi-walled morphology with diameters of 10 – 15 nm. Figure 2.2 shows a schematic of the 3-roll-mill calendering apparatus used to disperse CNTs (EXAKT 80E, EXAKT Technologies, USA) and lists the key processing parameters.

The process involved passing a batch of 80 to 120 g VE monomer/CNT mixture from the collector plate back to the material feed section while periodically decreasing the roller gap settings. A calendaring run consisted of 5 passes at 25 μm , 10 passes at 15 μm , and 20 passes at 5 μm . This procedure was developed previously [31] and ensured a high dispersion of CNTs in the VE monomer. The mixing in of styrene monomer at 40 wt% was accomplished using a hand-held homogenizer (Tissuemiser Homogenizer, Fisher Scientific, USA). Final CNT concentrations ranging from 0.1 to 1 wt% were prepared for fiber reinforced panels and bulk resin specimens using this method.

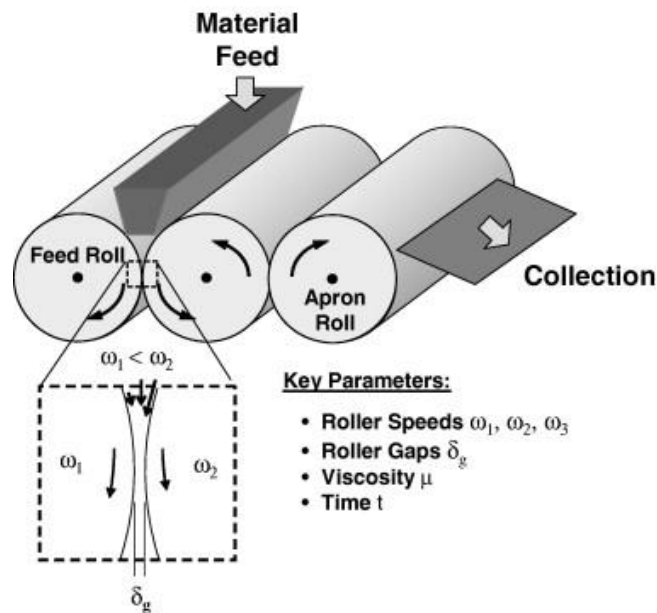


Figure 2.2: Schematic of 3-roll-mill showing key parameters of the high shear mixing process [31]. Reproduced with permission from Elsevier.

2.3 Dispersion by Functionalization and Ultrasonication of Carbon Nanotubes

To achieve dispersion in vinyl ester resin without the use of the calendaring method, CNTs were oxidized in a dilute solution of ultra-pure deionized water (1 g/L CNT concentration) while undergoing ultrasonication and ozone treatment using a previously developed method [32]. It was expected that an oxygen-rich surface functionality would aid the dispersion of CNT in the VE resin system. A schematic of the apparatus used is shown in Figure 2.3. A peristaltic pump (MU-D01, Major Science, USA) was used to circulate the CNT solution through a sonicator cell (Sonicator 3000, Misonix, with 800B Floccell, Qsonica, USA) and into a 2 L Erlenmeyer flask with ozone gas bubbler. Ozone gas was produced by corona discharge with an oxygen-fed ozone generator (1000BT-12, Taoture International Enterprises Inc, China). Both the sonication cell and Erlenmeyer flask were kept in circulating water set to 5 °C. Using the reported x-ray photoelectron spectroscopy (XPS) results of An and co-workers in Ref. 32, the total treatment time of six hours would have resulted in an oxygen-to-carbon ratio of about 0.09, compared to 0.02 for untreated CNT.

The CNTs were extracted from the dilute solution using an electrophoretic deposition (EPD) process onto stainless steel plates. An electric field strength of about 30 V/cm was applied for 2 hr. This caused the CNTs to collect onto the electrode plates and fall out of solution. The product was dried overnight on a hot plate at 80 °C. A 50 % yield of the original CNT mass was achieved. To disperse the oxidized carbon nanotubes in vinyl ester resin, the CNTs, with a few drops of styrene monomer, were briefly milled in a mortar and pestle to break apart the wafer-like product into smaller agglomerates. The styrene prevented the liberation of CNT particles into the air. The product was then added to the VE and styrene mixture

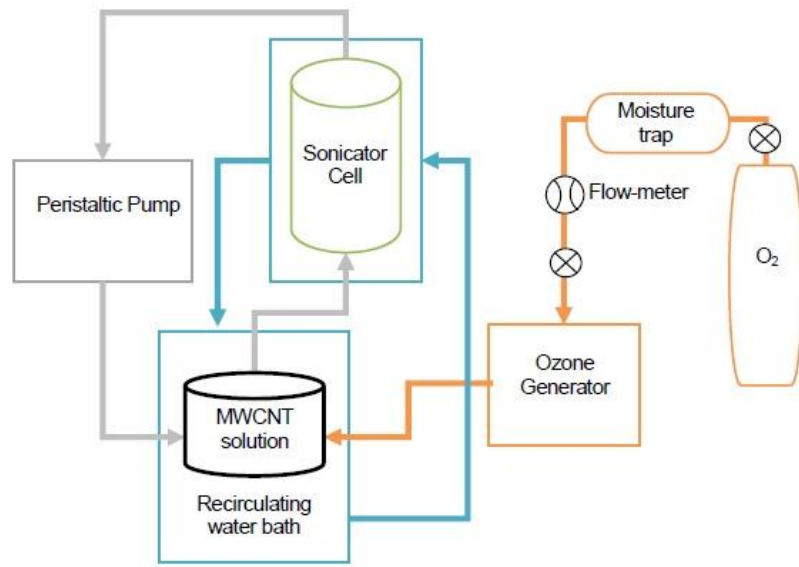


Figure 2.3: Diagram of apparatus used to oxidize and sonicate carbon nanotubes [32]. Reproduced with permission from Elsevier.

and placed in a sonication bath (Model Branson 1510, Emerson Industrial Automation, USA) for three hours. Small quantities of resin (~ 10 g) with CNT concentrations ranging from 0.1 wt% to 1 wt% used in the cure monitoring experiments were prepared using this method.

2.4 Fabrication of Multifunctional Fiber-Reinforced Composites

To fabricate structural composites of glass fiber and CNTs dispersed in vinyl ester resin, a vacuum assisted resin transfer molding (VARTM) method was used. The VARTM process is used to fabricate large complex geometry parts, especially in the marine industry, and is well suited for laboratory scale manufacturing. It is a low-cost method which can be used with a variety of tooling surfaces. The preparation for infusion of resin was as follows (reference Figure 2.4). First, a fiber preform was placed on the tooling surface which had been coated with a release-agent. Next, a

Teflon peel ply material was placed over the preform followed by distribution media. After placing the resin inlet and vacuum outlet tubes in place, the entire assembly was sealed with vacuum sealant tape under a layer of vacuum bagging material. In the step prior to infusion, vacuum was applied to check for leaks and to evacuate excess air from the preform and assembly.

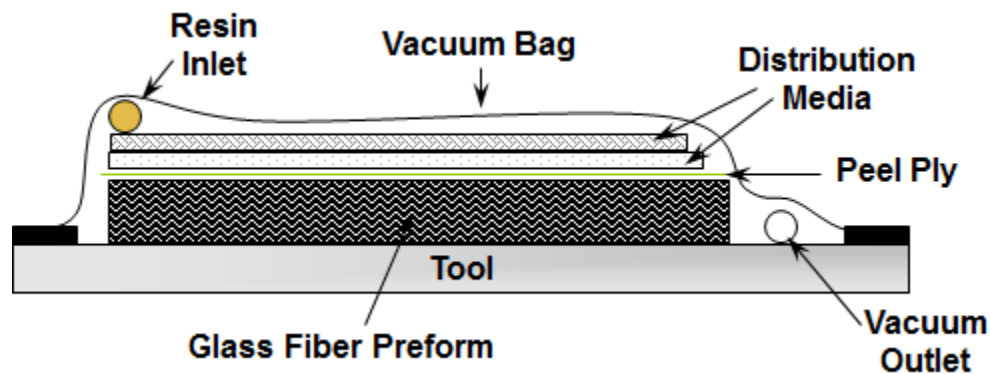


Figure 2.4: Schematic showing vacuum assisted resin transfer molding processing technique used to fabric multifunctional composites [22]. Reproduced with permission from American Chemical Society.

With the preform prepared for infusion, the curing agent and accelerator were mixed by hand into the CNT/VE resin for approximately 1 min. The inlet tube was then immersed in the resin and opened to allow the resin to flow into the fiber preform. A picture of an infusion a few moments after opening the inlet tube is shown in Figure 2.5. The distribution media allows much of the resin to flow over the top of the preform as vacuum pulls it through the thickness of the preform. Once the resin begins to enter the outlet tube, the inlet is closed and the excess resin is drawn from the preform. It is key that these steps are completed prior to resin gelation; otherwise

the part will not be completely infused, have excess voids, or will have too high a matrix volume fraction. After gelation, the vacuum tube was sealed off for the remainder of the initial curing phase.



Figure 2.5: Photograph of glass fiber preform being infused with vinyl ester resin with dispersed CNTs. Used with permission of E.T. Thostenson.

After curing overnight in the sealed bagging material, the panels were carefully demolded from the tooling surface and peel-ply material and placed in an oven set to 165 °C where they remained for 2 hr. This was the post-cure cycle determined from a differential scanning calorimetry (DSC) study [33] to give a complete reaction of the vinyl ester and styrene monomers.

Chapter 3

EXPERIMENT DESIGN AND INSTRUMENTATION

3.1 Combined Thermomechanical / Thermoresistive Analysis

3.1.1 Background

Several researchers have attempted to experimentally measure the effect of temperature change on the electrical properties of CNT filled polymers [34-43]. Typical experimental approaches measure DC resistance across a thin film or plate sandwiched between two cylinders with electrical contacts made within the material or on the cylinders. These methods may be an appropriate way to measure the electrical resistance of neat polymers at room temperature, but these methods fail to account for geometric factors such as particle size and dispersion, or thermal expansion. Because the specimens are typically constrained between two cylinders, the material is not able to expand and contract freely in all directions during heating or cooling. Furthermore, CNTs have very large aspect ratios and it is possible that a small number of CNTs or CNT agglomerates could span the thickness of these specimens, bringing into question the validity of using thin plates or films as test specimens in a through-thickness measurement. The results produced using these methods do not accurately represent the bulk electrical properties but are instead the result of statistically spanning clusters of CNTs. As a consequence there is wide variation in results reported in the scientific literature. In order to accurately measure bulk electrical properties, the specimen geometry and factors influencing electrical resistance should be considered. In

previous research [31] the parallel plate method per ASTM D257 [44] was found to be unreliable for dispersed CNT composites and a rectangular specimen was adopted. Other researchers have also adopted the use of rectangular specimens [34,40] to get accurate bulk resistivity measurements.

In this research, we evaluate the thermoresistive behavior of CNT/vinyl ester nanocomposites and establish an experimental approach where electrical resistivity is measured with volumetric expansion. The thermoresistive behavior of particle filled polymers or composites was assumed to be affected by the particle geometry and dispersion, particle electrical properties, polymer/interphase electrical properties and thermal expansion. The contribution of CNT thermoelectrical properties was expected to be minor given the distribution of metallic and semi-conductor behaviors recorded in the literature [12,45]. To characterize the thermoresistive behavior of CNT/vinyl ester composites the DC electrical resistance was measured *in situ* during thermomechanical analysis. The experiment was designed to allow for near-free volumetric expansion of the specimen while accommodating proven thermomechanical and electrical resistance measurements. Specimens ranging from 0.1-1 wt% CNT were thermally cycled for several hours in order to quantify the effect of temperature, thermal expansion, and thermal transitions in the polymer, as well as to observe any transient effects.

3.1.2 *In Situ* Electrical Resistance Measurements and Thermomechanical Analysis

Thermomechanical / thermoresistive analysis was conducted using a thermomechanical analyzer (TMA) (TMA/SDTA841e, Mettler Toledo, USA) with a multifunctional data acquisition device (NI-6218, National Instruments, USA)

controlled using customized LabVIEW software and an external PC. A minimum of 3 nanocomposite specimens of each nanotube composition were tested in order to ensure repeatability of the observed response. The specimens were designed specifically to meet the requirements of the TMA and also to accommodate an *in situ* electrical resistance measurement. Electrodes and lead wires were attached by first applying silver paint followed by silver filled epoxy to secure the lead wires to either end of the specimen. The conductive epoxy was cured at 60 °C for 2 hr.

Figure 3.1 shows the test configuration where the electrical resistance is measured along the length of the specimen and the TMA probe measures thermal expansion. As observed in Figure 3.1, the electrodes are not in contact with the TMA stage or probe and allow sufficient clearance from the environmental chamber when lowered into place. Specimens were then subjected to a total of nine cycles between 25 and 165 °C at a ramp rate of 3 °C/min. The electrical resistance was monitored during the entire testing period. The normal force exerted by the TMA probe was set to 1 N and 5 minute isothermal segments were programmed for 25 and 165 °C to enable the specimen to reach thermal equilibrium. The coefficient of linear thermal expansion (CLTE) given by the normalized derivative of specimen height (h) with temperature (T) given by $\left(\frac{10^6}{h_0}\right) \frac{dh}{dT}$ where h_0 is the initial specimen height at room temperature and the units are expressed as $10^{-6}/^{\circ}\text{C}$.

A diagram of the electrical circuit for the specimen resistance measurement and interface with the data acquisition device is shown in Figure 3.2. The electrical resistance was determined through Ohm's Law by measuring the voltage drop across the specimen and the reference resistor wired in series with an excitation voltage of 5 V. A two-probe measurement was used because the specimen resistance values were



Figure 3.1: Photograph of nanocomposite specimen mounted on the TMA stage for thermoresistive characterization.

extremely large as compared to the lead wire contact resistance. The reference resistors (VFR Series, Vishay Precision Foil, Israel) used were ultra-precise and extremely stable under varying conditions. A hermetically sealed reference resistor (VHP Series, Vishay Precision Foil, Israel) was used when measuring the 0.1 wt% specimens to improve the ultra-low current measurement stability. The reference resistor value was chosen to match the resistance range of the specimen type being tested. For example, the 0.1 wt% CNT/vinyl ester specimens had an average resistance of about 800 k Ω and the reference resistor was chosen to be 1 M Ω . By selecting a reference resistor within an order of magnitude of the specimen resistance, an accurate measurement was ensured. Table 3.1 shows the specimen resistance range and reference resistor used in the measurements. Electrical resistance is represented in normalized form by $\Delta R/R_0$ in %. The temperature coefficient of resistance (TCR) was

calculated in a similar way to CLTE and is the normalized derivative of resistance (R) with temperature given by $\left(\frac{10^6}{R_o}\right) \frac{dR}{dT}$ where (R_o) is the initial resistance at room temperature (unless otherwise noted) and the units are expressed as $10^{-6}/^{\circ}\text{C}$.

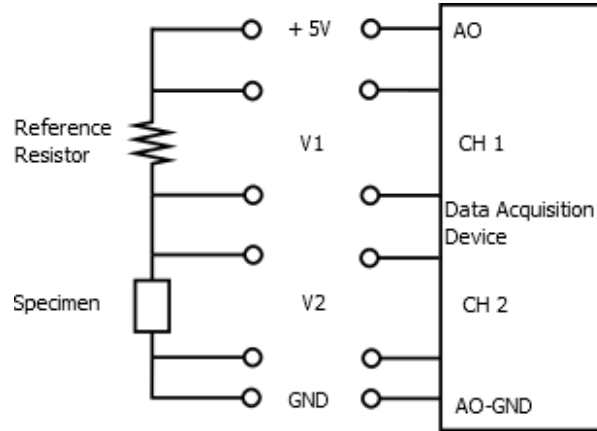


Figure 3.2: Electrical circuit and data acquisition interface diagram.

Table 3.1: Average electrical resistance range during thermal cycling and value of reference resistor used for each specimen group.

Carbon Nanotube Concentration (wt%)	Specimen Resistance Range (Ω)	Reference Resistor (Ω)
1.00	11,167 – 12,018	10,000
0.75	15,401 – 16,365	10,000
0.50	118,970 – 125,067	100,000
0.10	805,467 – 805,667	1,000,000

The specimen volume resistivity (ρ_v) at ambient temperatures can be calculated using the measured resistance, specimen cross sectional area (A) and specimen length (l), which represents the distance between the two electrodes.

$$\rho_v = R \frac{A}{l} \quad (3.1)$$

In the TMA measurement the height of the specimen is measured as the temperature is changed. Assuming that the thermal expansion coefficients (α) of the nanocomposites are isotropic, the specimen will expand proportionally in all directions and the area and length can be expressed as:

$$A = w_o(1 + \alpha(T - T_o))h \quad (3.2)$$

and

$$l = l_o(1 + \alpha(T - T_o)) \quad (3.3)$$

where w_o is the initial specimen width, l_o is the initial specimen length and T_o is the initial specimen temperature. For all specimens l_o and w_o are 13 and 3 mm, respectively. Substituting Equations (3.2) and (3.3) into Equation (3.1) we can calculate the volume resistivity based on the measured specimen height at any temperature by:

$$\rho_v = R \frac{w_o}{l_o} h. \quad (3.4)$$

Note that the coefficient of thermal expansion and temperature change are eliminated in Equation 3.4 since the proportional change in specimen width and length is the same with temperature.

3.2 *In Situ* Measurements during Environmental Testing

3.2.1 Background

Aerospace applications increasingly demand reduced weight, higher performance and lifetime durability from their constituent materials. Materials used in these applications must meet strict design requirements over an extreme temperature range. Multifunctional composites of CNTs will likely be utilized in future airplanes and spacecraft as a means of monitoring both the short-term and long-term material

changes through *in situ* damage sensing and health monitoring. It is therefore critical that experimental methods are developed to evaluate multifunctional materials under extreme environments. The work of Gates and Whitely [2,46,47] has presented many useful methodologies and experimental data for the evaluation of composite materials in extreme environments. Their approach was adopted in this study to evaluate the performance of glass fiber/CNT/VE composites under a combined mechanical and thermal loading.

3.2.2 Instrumentation

Cross-ply composites of glass fiber and dispersed CNTs in vinyl ester resin were tested under combined thermal and mechanical loading during prolonged thermal cycling. The electrical resistance of the specimens was monitored *in situ* and in real-time using a data acquisition system. Specimens were placed in a constant displacement weathering fixture originally design by NASA for evaluating the performance of polymer composites at cryogenic temperatures [46], and pre-strained to approximately 1300 $\mu\epsilon$, roughly 45 % of typical tensile strain to damage initiation values. The fixture, shown in Figure 3.3, was made of a special Invar alloy which has a near zero thermal expansion coefficient. The end tabs served the additional purpose of electrically insulating the specimen from the weathering fixture during electrical resistance measurements. The assembly was placed inside an environmental testing chamber (Z8-Plus, Cincinnati Sub-Zero, USA) and cycled using the maximum performance limitations of the chamber. Edge replicas were taken before and after pre-straining, and again after the tests were completed to track the progressing of damage.

The thermal cycling profile consisted of 30 minute isothermal segments for the temperature extremes of 150 and -73 and also 25 °C. Although relative humidity had a set point of 5 %, the humidity varied greatly during the heating and cooling ramps because the high ramp rates. A typical temperature/humidity profile for a single cycle is shown in Figure 3.4. The influence of moisture absorption on the electrical resistance of this material system has not been determined at this point; however, it is assumed to have had a negligible effect given the relatively short periods of high humidity exposure. A total of 13 thermal cycles were completed in 56 hr and the changes in electrical resistance were monitored continuously over the duration of the test.



Figure 3.3: Constant displacement weathering fixture used for environmental testing of composites.

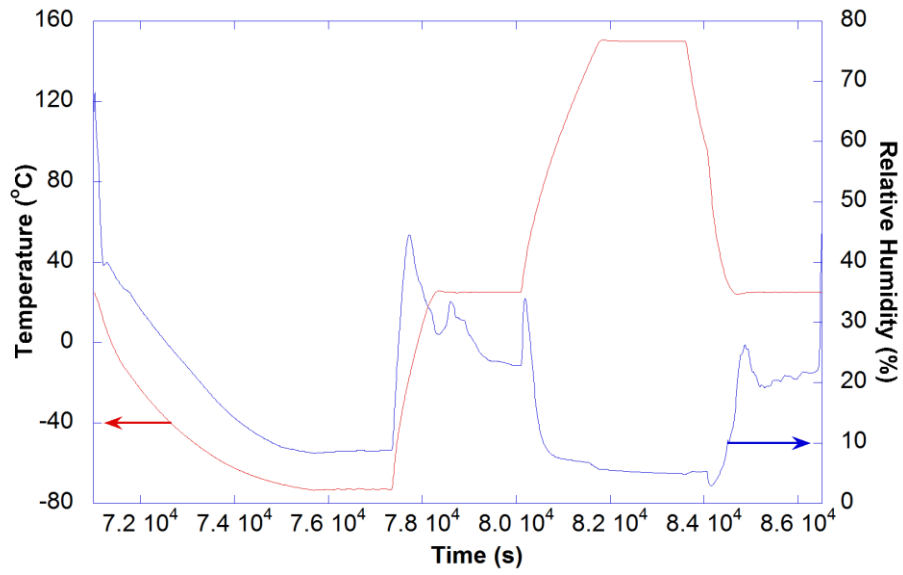


Figure 3.4: Typical temperature and humidity profiles during a thermal cycle.

The data acquisition system used for environmental testing was composed of National Instruments signal conditioning cards with a NI-PCI card and Keithley 6430 and 2182A voltage/current meters. The system is capable of measuring a single resistance channel, two strain channels, and an acoustics emissions channel in real-time. The 2182A is used when making resistance measurements of highly conductive carbon fiber composites. The streaming data are presented on a custom LabVIEW program as the test progresses and stored to a spreadsheet for later analysis. The entire system is contained in a mobile computer station. Temperature and humidity data were collected and stored by the CSZ environmental chamber. The data sets were combined before further data reduction and analysis. The latest expansion of this system included a Keithley multiplexer/multimeter device which will be used for the identification of damage location during testing.

3.3 *In Situ* Electrical Resistance Measurements during Torsional Braid Analysis

3.3.1 Background

Variability in resin chemical make-up and in manufacturing conditions result in a degree of uncertainty during processing of composite materials. Also, because of the inherent anisotropy of fiber reinforced composites, residual stresses form during the curing process which can cause deformation and poor performance in the finished product. Unfortunately, the current usage of quality control and process optimization rely on probability, whereas a higher degree of certainty is required for critical structures in aerospace and marine applications. There is a need to develop practical and scalable methods of *in situ* process monitoring.

The sensing mechanism for composites of dispersed CNT is believed to have its origin in the CNT-CNT interphase region which is occupied by the polymer matrix. For this reason the electrical resistance sensing technique should be sensitive to polymer electrical properties which are known to change during cure. In this work, a novel process monitoring technique was developed with the goal of extending the sensing functionality of the dispersed CNT material system into the processing phase of composite materials manufacturing. To demonstrate the proposed sensing method, the torsional braid analysis (TBA) method was adopted. The method allowed for an *in situ* electrical resistance measurement during viscoelastic measurements of the curing processes of a composite.

Because of its high sensitivity to morphological changes in thermosetting materials, torsional braid analysis has been used to study cure and transformation phenomena in many resin systems, including epoxy and vinyl ester systems [48-50]. In torsional braid analysis, a glass fiber braid is saturated in resin and allowed to cure

under isothermal or continuous heating conditions while monitoring changes in the damping of an induced oscillation [51]. In this study, a rheometer with a torsion accessory was used as an analog for the traditional TBA apparatus, and the electrical resistance of the TBA specimen was monitored during torsional braid analysis.

3.3.2 Instrumentation

A rheometer (AR-2000, TA Instruments, USA) with solid geometry torsion accessory was used as an analog for the torsion pendulum (Figure 3.7). Instead of measuring the frequency and damping of an intermittently induced oscillation, as in traditional TBA experiments, a continuous oscillation of fixed angular displacement and frequency was applied to the specimen [51]. During cycling torsional loading, a phase lag between shear strain and stress is produced, giving rise to a complex shear modulus where $G = G' + iG''$. G' is known as the storage component and is a measure of stiffness and G'' is the loss component and is a measure of dissipated mechanical energy. The rheometer compares the source and response waveforms to calculate the relative storage and loss moduli and delta, defined by $\tan^{-1} G''/G'$. Isothermal and temperature ramp segments were run at 0.0314 rad displacement at 1 Hz with ramping rates of 2 °C/min and a normal force of 0.5 N (+/- 0.3 N) tension. The three temperature profiles used are shown in Figure 3.5. Profiles I and II begin with a 2 hour isothermal cure segment followed by a 2 or 1 hour post-cure step. Profile III has a continuous heating cure segment followed by a 2 hour post-cure step. All profiles include thermal cycles in order to measure the thermoresistive and viscoelastic trends following the curing steps.

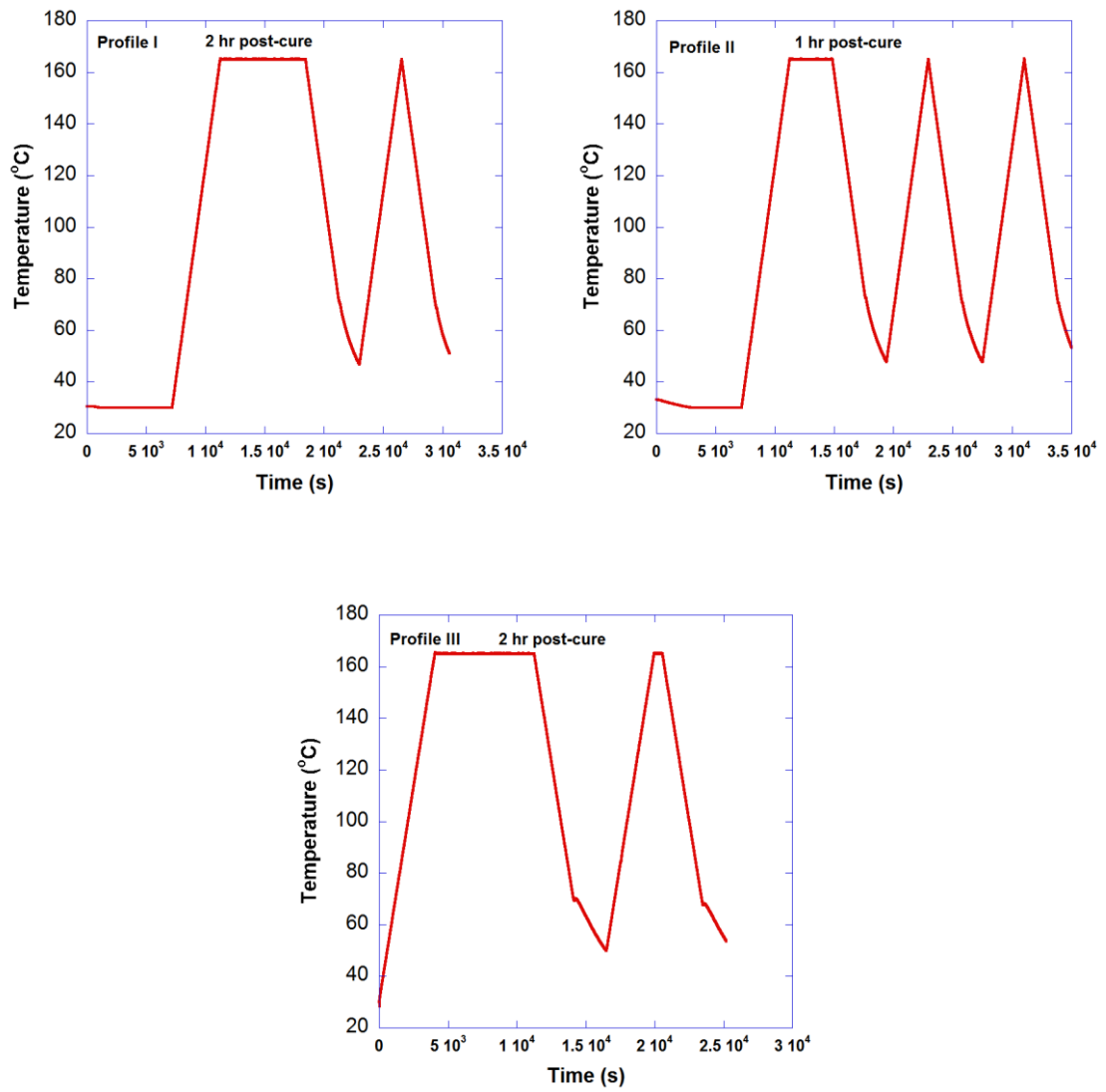


Figure 3.5: Temperature profiles used during torsional braid analysis.

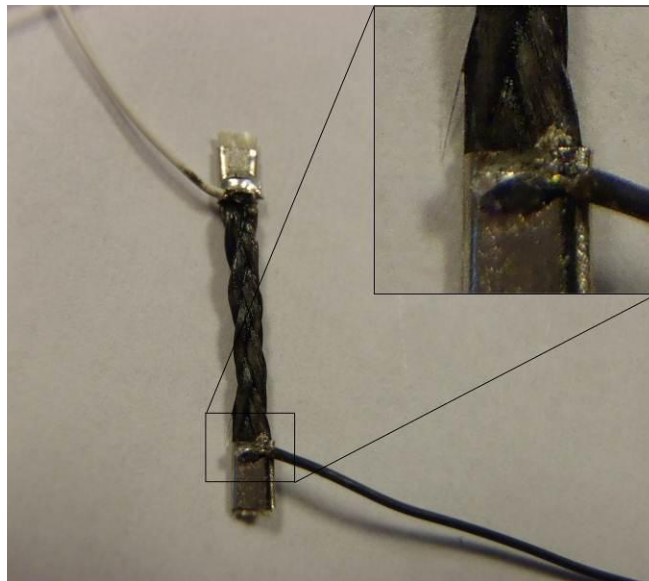


Figure 3.6: Image of a 0.25 wt% CNT/VE TBA specimen showing zoom in of electrode area.

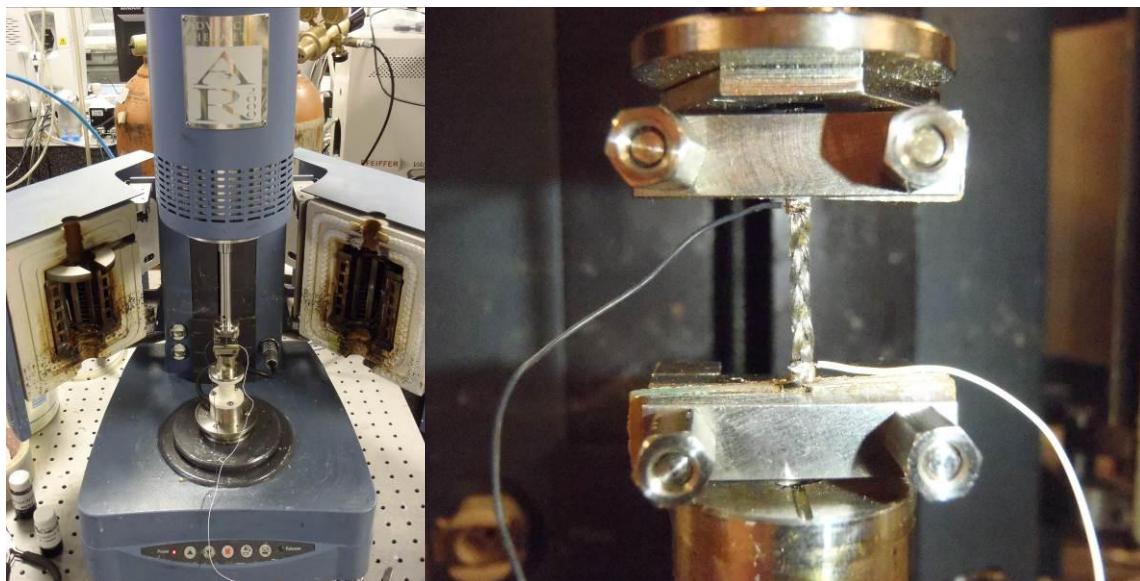


Figure 3.7: Images of TBA set-up, left; AR-2000 rheometer with Environmental Testing Chamber (ETC) and torsion accessory attached, right; torsion clamp with 0.1 wt% CNT/VE specimen mounted.

The specimens were prepared using a glass fiber braid consisting of three twisted-pair tows in a normal braid pattern. The ends of the braid lengths were secured using a 1 mm ID nickel crimp tube, which also served as the electrode during electrical measurements. A gage length of 13 mm was found to provide sufficient torsional stiffness for the tests. For some experiments, a drop of conductive silver paint (SPI Flash-Dry™ Silver Paint, SPI Supplies Inc., USA) was applied to the braid ends just prior to securing the nickel tube in place to improve the electrical contact. Ultra-fine, 36 awg silicone coated wires (SiliFlex, Calmont Wire and Cable, Inc., USA), used to minimize interference with the rheological measurement, were soldered to the nickel crimp tube to make lead wires for electrical measurements (Figure 3.6). An ultra-high precision hermetically sealed reference resistor (VHP101, Vishay Precision Group, USA) was used with the data acquisition set-up described in Section 3.1.2. Images of the rheometer set-up are shown in Figure 3.7. After loading the specimen into the rheometer, two drops of resin were placed on the glass braid substrate and allowed to saturate the fibers before running the rheometer and data acquisition programs.

Chapter 4

THERMORESISTIVE CHARACTERIZATION OF CARBON NANOTUBE/VINYL ESTER COMPOSITES

4.1 Results and Discussion

4.1.1 Thermoresistive Response under Thermal Cycling

Previous research [31] showed that the electrical percolation threshold for CNT/vinyl ester nanocomposites was below 0.1 wt%. For the thermal cycling experiments the compositions were chosen to examine the thermoresistive response both near the percolation threshold and far above the electrical percolation threshold. Variability in initial resistance values for all the specimen groups were small. Figure 4.1 shows the typical observed transient electrical response under thermal cycling for the different nanocomposite compositions. The nanocomposite specimens that are well above the percolation threshold, 0.5-1 wt% showed fluctuations in the electrical resistance during the ramp up and ramp down segments of the thermal cycles but the trend observed is an increase in electrical resistance with increasing temperature and a decrease in resistance upon cooling. In contrast, the 0.1 wt% CNT/vinyl ester specimens showed a decrease in the electrical resistance with increasing temperature, but the magnitude of the resistance change with temperature is orders of magnitude smaller than the other specimens. In addition, the 0.5 through 1 wt% CNT/vinyl ester nanocomposites showed an increase in average electrical resistance over time.

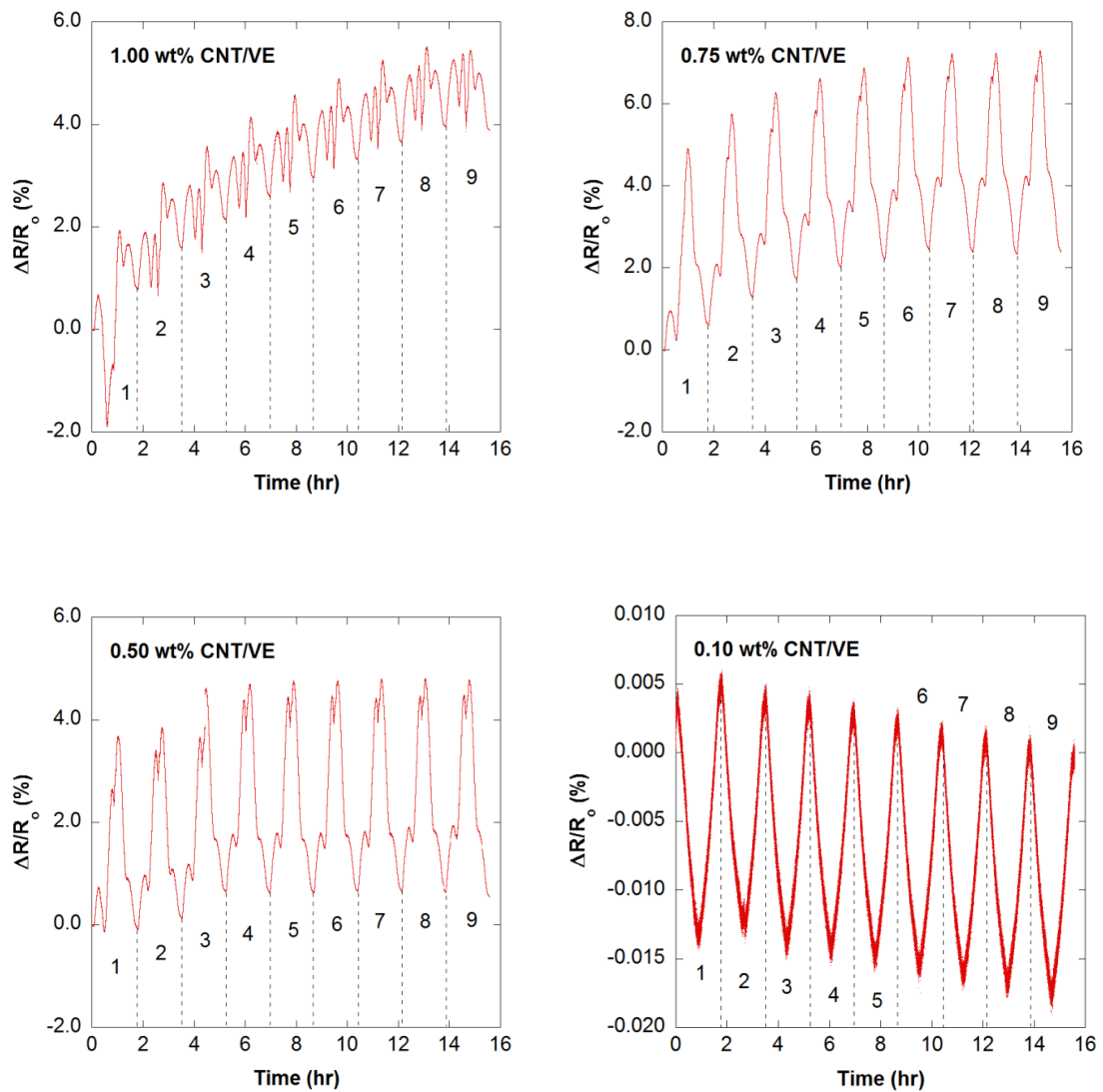


Figure 4.1: Normalized electrical resistance change of CNT/VE composites during iterative thermal cycling from 25 to 165 °C; dashed lines and numbering showing thermal cycle iteration.

In order to better visualize the effect of temperature and cycle iteration on electrical resistance, the electrical response is shown with respect to temperature in

Figure 4.2. Note that the data for the 0.1 wt% CNT/vinyl ester specimen was filtered in order to clearly resolve the small cycle-to-cycle changes. In this case, additional signal processing was required because the relative noise amplitude was large compared with the resistance changes. For all other specimens the raw data is presented. In Figure 4.2 the 0.1 wt% nanocomposite shows an extremely small decrease in the electrical resistance with increasing temperature whereas the other nanocomposite compositions show a distinct shape to the resistance change / temperature curves with local maxima near 70 and 150 °C. In addition, the 1 through 0.5 wt% CNT/vinyl ester specimens clearly show increasing resistance during the 5 minute isothermal segments at 165 °C. This magnitude of the resistance change corresponds to an offset in the resistance change at 25 °C. As the number of thermal cycle iterations increased, the transient increase in resistance at 165 °C diminished. This transient behavior indicates that some permanent material changes are taking place at the high temperature isothermal segments. In order to show the permanent changes in resistance observed for 0.5 through 1 wt% CNT/vinyl ester specimens, the data from the 5 minute isothermal segments at 165 °C are plotted against total isothermal time in Figure 4.3. While some of the changes in resistance during each isothermal segment are due to thermal effects of the specimen reaching equilibrium, there is a clear overall trend in the data in a diffusion-like fashion.

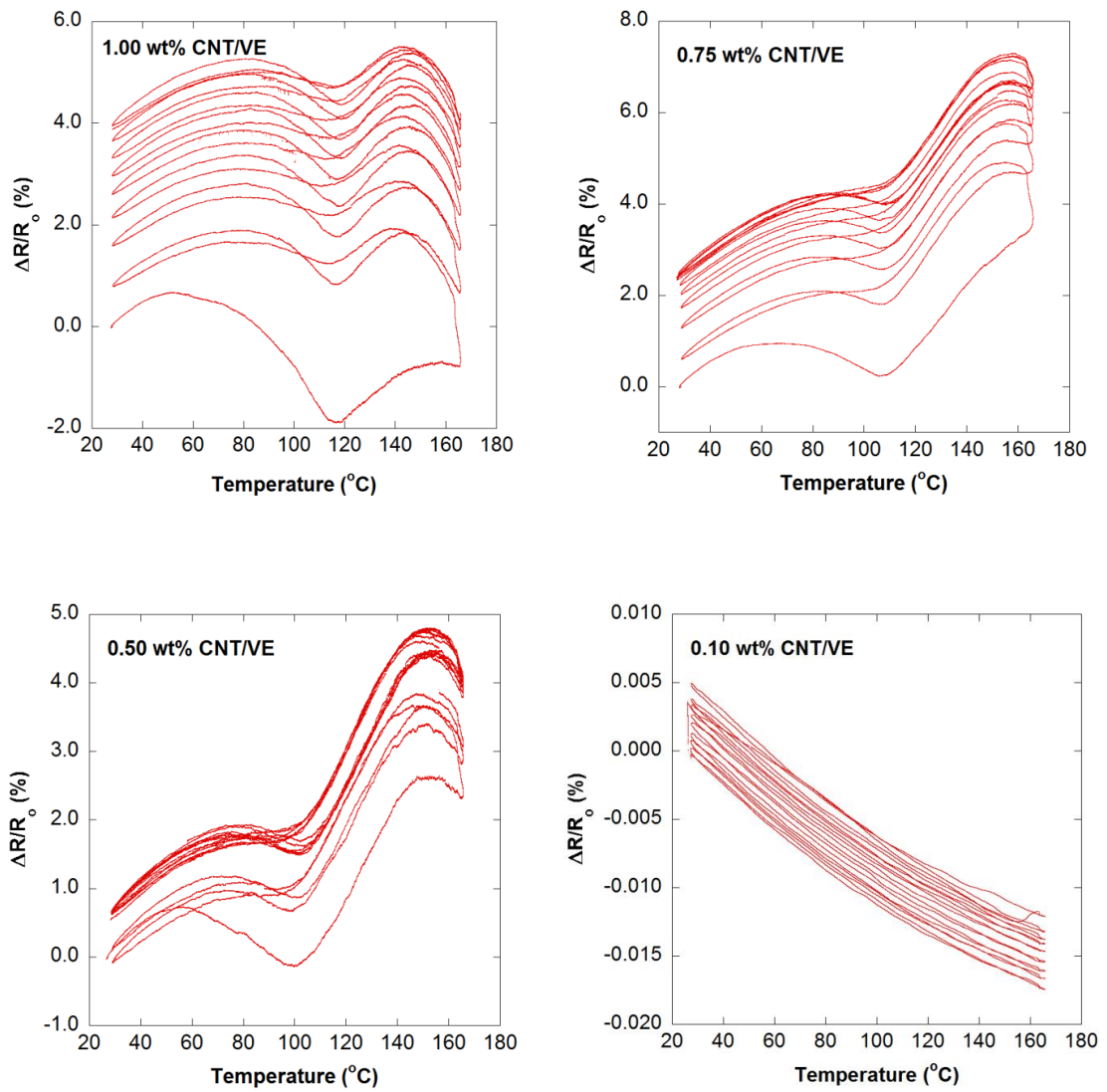


Figure 4.2: Normalized electrical resistance change versus temperature of CNT/VE composites during thermomechanical testing.

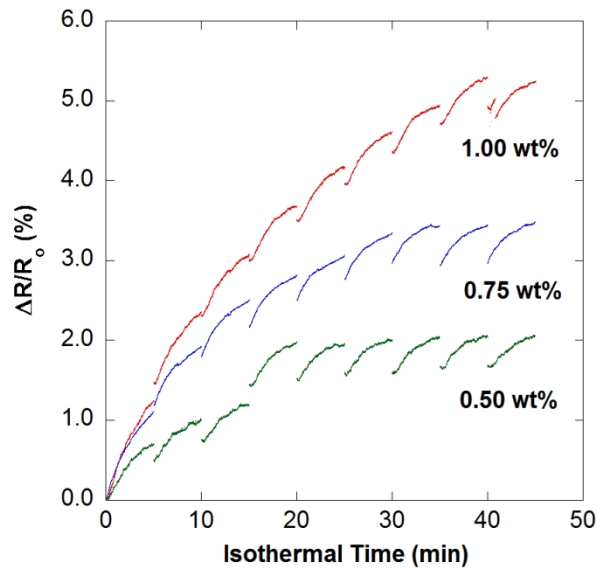


Figure 4.3: Normalized electrical resistance change during the isothermal segments at 165 °C showing diffusion-like increase in overall resistance (R_0 taken at initial 165 °C set-point).

After gelation, the later stages of cure become diffusion-limited and the reaction slows because the mobility of unreacted monomer is hindered by the formation of crosslinks. The post-cure cycle for the vinyl ester matrix was determined by a previous kinetic study [33] using differential scanning calorimetry (DSC). The slight increase in degree of cure at much later stages is difficult to measure during DSC because little exothermic heat is generated from the reaction during this time. For the vinyl ester system it is likely that styrene conversion continues to increase after most of the vinyl ester has reacted. As discussed earlier, the carbon nanotube network electrical conductivity is dominated by the tunneling resistance at the CNT/CNT junctions. The ability to detect this transient response during the isothermal segments is likely due to the local changes in the ionic conductivity of the polymer in the regions of the CNT/CNT junctions as material continues to react. As a

result, the numerous CNT/CNT junctions in composites well above the electrical percolation threshold become a distributed network of *in situ* cure sensors throughout the polymer matrix allowing the opportunity to detect chemical changes in the matrix. Although the specimens were post-cured for 2 hr these results indicate that the cure cycle determined by DSC results in an incomplete reaction.

4.1.2 Thermomechanical / Thermoresistive Analysis

Considering the transient phenomena observed during the thermal cycling experiments, the data from the final ramp-up segment was isolated for further analysis. The resistance change / temperature curve for the final thermal cycle are shown in Figure 4.4. Denoted on the plots are the locations of the local minima of interest. It was found that, for composites of 1 wt% CNT/vinyl ester, the electrical resistance increased from 25 to 80 °C, then decreased until 118 °C and increased again until 145 °C before decreasing steeply to 165 °C. This behavior was similar for the 0.75 and 0.5 wt% CNT/vinyl ester specimens, although less exaggerated. The resistance of 0.1 wt% CNT/vinyl ester specimens decreased monotonically with temperature, very different than composites with higher CNT content. Given that the percolation threshold has been experimentally observed to be less than 0.1 wt% CNT content for highly dispersed systems [31] as well as predicted by three-dimensional modeling [52], this difference in behavior indicates that as the number of CNT/CNT junctions increase with nanotube content, the thermoresistive behavior becomes increasingly sensitive to the polymer interphase or tunneling medium. This supports the predictive modeling work on CNT-reinforced composites which assumed a tunneling dominant resistance / strain response [30].

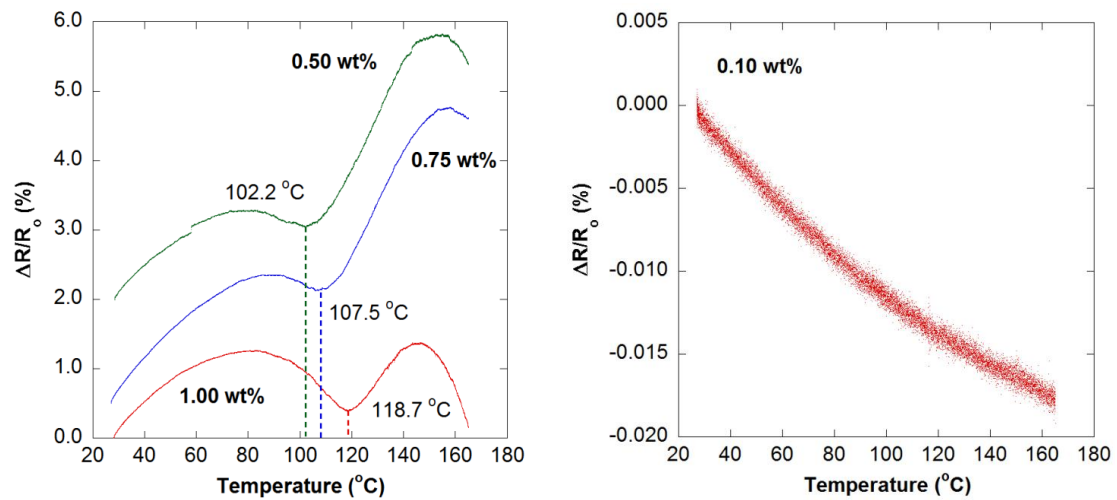


Figure 4.4: Electrical resistance change of CNT/VE composites during the final ramp-up segment; right: unfiltered data for 0.1 wt% specimen, left: local minima indicating T_g locations for specimens with greater than 0.1 wt% CNT (note that 0.5-0.75 wt% data are offset by 2 and 0.5 % resistance change, respectively, to clearly show the curves).

It was expected that thermal expansion is a major factor in the thermoresistive behavior of composites of dispersed CNTs. The data presented in Figure 4.4 does not account for dimensional changes in the specimen upon heating. The CLTE of the specimen changes as the polymer undergoes thermal transitions, particularly at the glass transition temperature (T_g). Figure 4.5 shows the dimensional change and CLTE for the 1 wt% nanocomposite. Around 120 °C there is a significant change in the slope of the expansion curve resulting at the glass transition temperature. In TMA, T_g is taken to be at the location where the dimension curve increases slope dramatically (inflection point in CLTE curve) and is considered to be the onset of polymer segmental or main chain motion [53]. This is the transition from the glassy to rubbery

state. The local minima in electrical resistance shown in the left of Figure 4.4 corresponded very closely with the glass transition measurements from the thermomechanical method. This was observed for all specimens with CNT concentrations well above the percolation threshold. To summarize the difference in T_g sensing methods, the values determined from the TMA and thermoresistive methods are presented in Table 4.1. The thermoresistive method yielded average glass transition temperatures 2 to 6 °C higher than the TMA approach, but had similar precision.

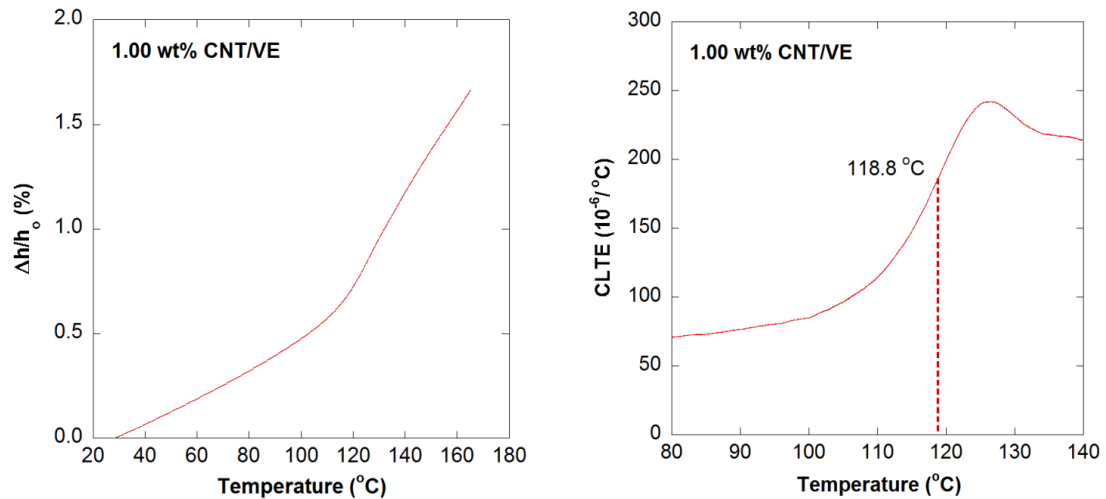


Figure 4.5: TMA results for 1 wt% CNT/VE specimen showing dimensional changes during heating and the calculated linear thermal expansion curve showing the T_g location.

Based on the coupled measurement of thermal expansion and resistance the volume resistivity of the nanocomposite can be evaluated as a function of temperature. Figure 4.6 shows the volume resistivity and expansion of the nanocomposites during

the ramp-up segment of the last cycle. The importance of thermal expansion is illustrated by comparing the shapes of the resistivity and expansion curve. Essentially, the larger the effect of thermal expansion, the more closely the resistivity curve resembles the expansion curve. The plot in Figure 4.6 for the 0.1 wt% CNT/vinyl ester specimen is a good example. Here, the resistance change with temperature was nearly constant; therefore, the resistivity was nearly proportional to the thermal expansion. For the nanocomposites well above the electrical percolation threshold the overall shape of the curve is similar to the measured resistance, with clearly defined maxima and minima. When volumetric expansion is taken into account it is clear that other mechanisms are contributing to the change in the material electrical properties with temperature. The local minima in both the resistance and resistivity curves in Figures 4.4 and 4.6 correlate strongly to the T_g measured by TMA (see also, Table 4.1). The locations of T_g varied with CNT loading but were consistent within each batch, as expected. Because each material type is synthesized and prepared at different times, batch-to-batch variation is likely the origin of the differences. As a result, the thermoresistive analysis of the carbon nanotube network enables *in situ* measurement of glass transition in a bulk material without the use of complex thermal analysis instrumentation.

Table 4.1: Comparison of the thermoresistive and thermomechanical methods for sensing T_g showing the average of three specimens.

Carbon Nanotube Concentration (wt%)	T_g – Thermoresistive Method (°C)	T_g - Thermomechanical Method (°C)
1.00	115 ± 2	113 ± 3
0.75	109 ± 2	105 ± 2
0.50	102 ± 3	96 ± 3

The temperature coefficient of resistance is analogous to the thermal expansion coefficient and is a measure of a material's electrical resistance response to temperature change. Figure 4.7 shows the variation in TCR with temperature for the various nanocomposites. Note that the 0.5 through 1 wt% CNT/vinyl ester nanocomposites share a common shape of the resistance change versus temperature curve (Figure 4.4). This is reflected in the similarity between their respective TCR curves. Clearly, for these material types, TCR varied widely over the temperature range and is positive or negative over the span from 40 to 160 °C. The 0.75 wt% CNT/vinyl ester specimens had the highest degree of sensitivity to temperature, a peak TCR of roughly $2,400 \text{ } 10^{-6}/^{\circ}\text{C}$. The TCR range of the 1 and 0.5 wt% CNT/vinyl ester materials had similar values. In contrast, the 0.1 wt% CNT/vinyl ester specimens had an extremely low and negative TCR, an average value of $-1.2 \text{ } 10^{-6}/^{\circ}\text{C}$ over a 120°C span. There were no significant changes in the TCR trend in the T_g region for this material.

The results show that for the specimens far above the percolation threshold that influences other than thermal expansion strongly affect the electrical resistance signal. For the 1 wt% CNT composite the variations in electrical properties are most pronounced while composites with lower concentrations of CNTs show electrical responses that are more influenced by thermal expansion. With volumetric expansion of the polymer matrix the tunneling gap between the individual nanotubes expands while, on the other hand, an increase in temperature increases the electron mobility. At lower nanotube concentrations there are fewer tunneling gaps and the thermal expansion more strongly dominates this effect. At higher nanotube concentrations there are not only more CNT/CNT junctions but it is likely that, on average, the

tunneling gap between nanotubes is smaller enabling thermally-activated hopping of the electrons. As a consequence the resistance measurements are more sensitive to thermal transitions in the polymer where changes in segmental mobility affect the tunneling of electrons.

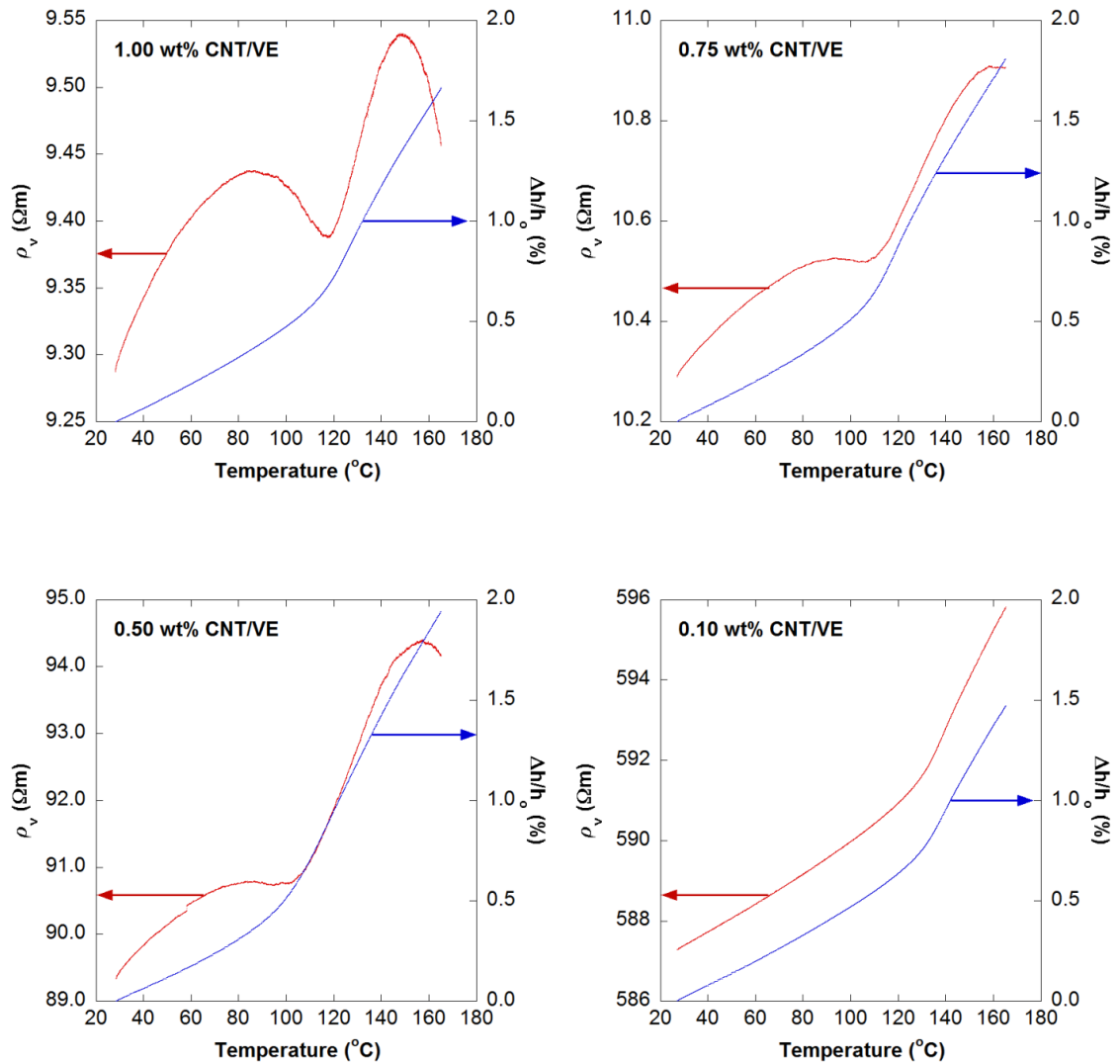


Figure 4.6: Comparison of volume resistivity and dimensional change curves for CNT/VE composites during final ramp-up segment.

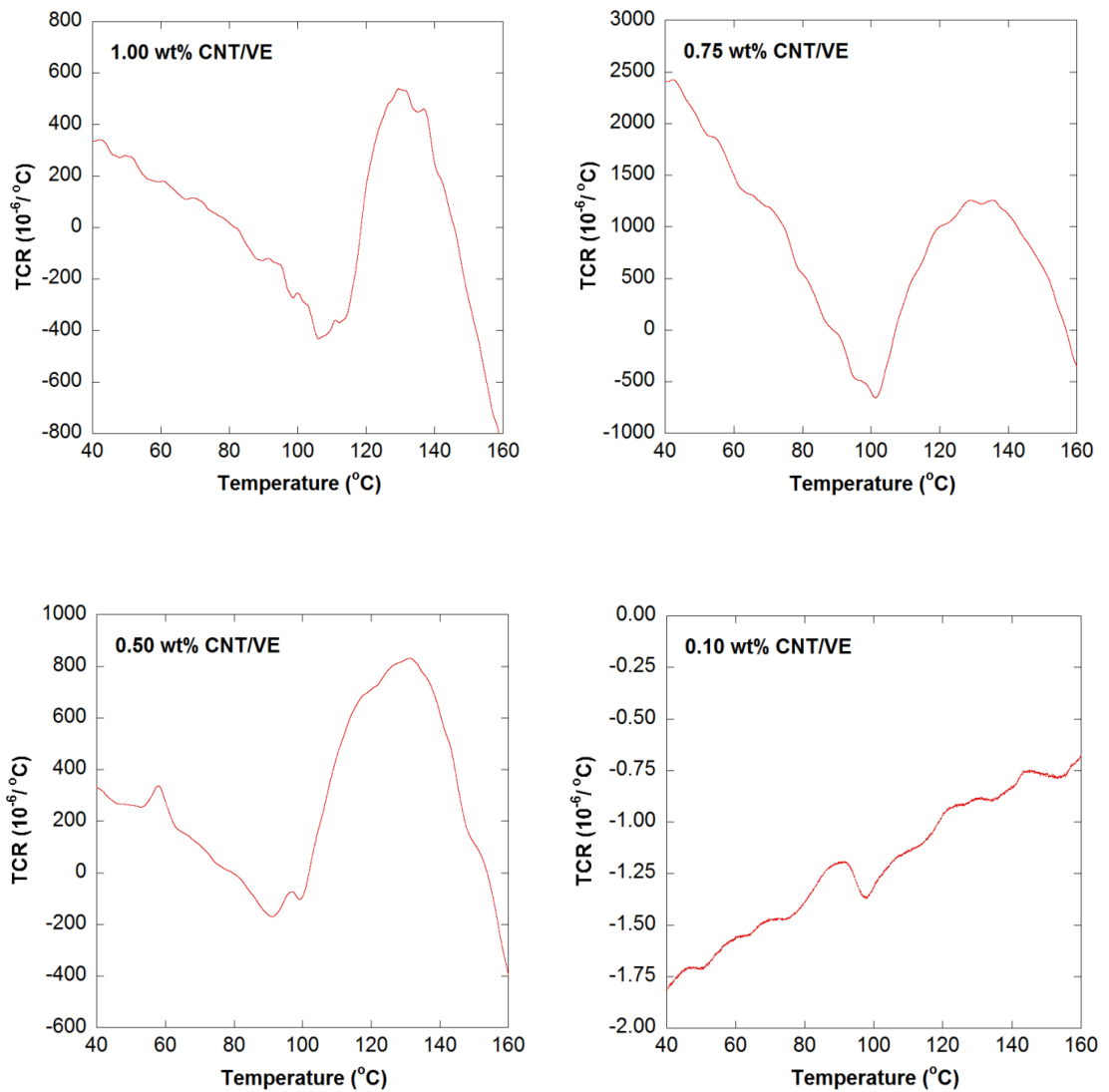


Figure 4.7: TCR curves for composites of CNT and vinyl ester during final ramp-up segment showing difference in thermoresistive trends for 0.5-1 versus 0.1 wt% composites.

In the study of thermoelectrical properties of polymers, electrothermic analysis methods such as the thermally stimulated discharge current method (TSD or TSDC)

have been used to study carbon black-filled polymers [54] and more recently to study nanocomposites [55]. TSDC is very sensitive to variations in the dielectric properties which are related to specific side-chain and segmental processes including the γ , β , α (T_g) and ρ processes [56]. Goel and co-workers [57] used TSDC to investigate the electrical properties of vinyl ester and observed similar trends in local maxima in the dielectric constant to peaks observed in thermoresistive analysis using CNTs. The CNT/CNT junctions with a thin region of vinyl ester between the contacts act much like a nanoscale electrothermic sensor. As a result the percolating structure of the nanotubes may also act as a distributed network to sense polymer transitions.

4.1.3 Summary

The thermoresistive behavior of composites of CNTs and vinyl ester was determined by measuring electrical resistance *in situ* during thermomechanical analysis. The thermomechanical analyzer allowed for the thermal expansion to be accounted for in the calculation of volume electrical resistivity which provided additional insight that would otherwise have been ignored. Of the factors assumed to affect the thermoresistive behavior of CNT filled polymers, the results showed that CNT concentration, polymer/interphase electrical properties and thermal expansion had the greatest effects. The latter two of these factors are strongly dependent on temperature and polymer thermal transitions. The 0.1 wt% CNT nanocomposite had a near-zero and negative TCR whereas specimens with greater CNT loading had positive and negative TCR. Specimens with 0.5 to 1 wt% CNT (well above the percolation threshold) showed sensitivity to changes in the polymer interphase apart from thermal expansion. The glass transition was accurately detected in these specimens by taking the local minimum in the electrical resistance / temperature

curve. It was shown that tunneling-based sensing using CNTs could detect transient effects resulting from further cure even beyond that of the DSC method.

Thermoresistive analysis using CNTs was found to be similar to a much more complicated electrothermic analysis technique, the TSDC method. In composites of dispersed CNTs, the tunneling of electrons across CNT/CNT junctions gives rise to a network of sensors formed by a percolating network of nanotubes.

Chapter 5

COMBINED THERMAL AND MECHANICAL LOADING OF COMPOSITES OF GLASS FIBER/CARBON NANOTUBE/VINYL ESTER

5.1 Results and Discussion

5.1.1 Pre-Tensioning of Composite Specimens

Electrical resistance and the longitudinal and transverse strains were monitored during the pre-tensioning step prior to starting the environmental chamber's thermal cycling profile. The typical data for this step are shown in Figures 5.1-2. Here, the changes in the resistance and strain are caused by the turning of the manual tensioning mechanism. In Figure 5.2, the normalized electrical resistance data for four specimens are plotted with respect to longitudinal strain. Two of the specimens experienced damage initiation during this step as marked by the large vertical gaps between data points. The figure shows the typical resistance / strain response observed during quasi static tensile tests of this material [58] (see Section 1.6). In the linear elastic region, electrical resistance generally increases in a linear fashion with tensile strain. Step-like increases in resistance are caused by crack formation.

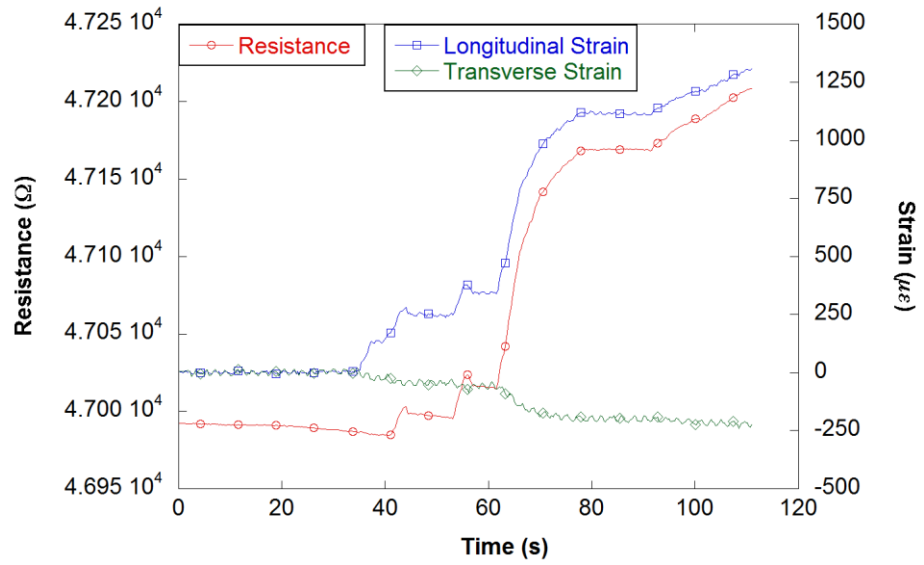


Figure 5.1: Pre-tensioning step: typical time lapse showing electrical resistance and longitudinal and transverse strains.

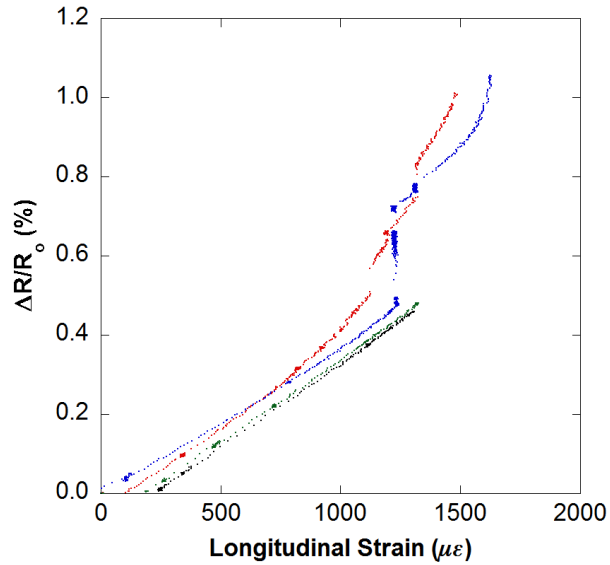


Figure 5.2: Normalized electrical resistance change of four specimens versus longitudinal strain during manual tensioning of specimens inside of weathering fixture.

5.1.2 Sensing of Stress Relaxation and Damage during Environmental Testing

A typical electrical resistance trend over the duration of the environmental testing is shown in Figure 5.3. The electrical resistance decays, reaching equilibrium after 7 to 9 thermal cycle iterations. The noisy areas apparent in the first few thermal cycles are attributed to water condensing on the specimen surface during the warm up from $-73\text{ }^{\circ}\text{C}$, providing a kind of short circuit. It is interesting to note that as the test progresses, the noise in this region trends toward zero as the moisture content of the chamber air is reduced further which each thermal cycle. It was not uncommon to observe frost melting from the weathering fixture during the ramp up from low temperatures. Also notable is the difference between the resistance values at the end of each of the $25\text{ }^{\circ}\text{C}$ isothermal segments. This value was consistently higher upon returning to 25 from $-73\text{ }^{\circ}\text{C}$ than from $150\text{ }^{\circ}\text{C}$. This may be due to thermal history formed during the low temperature segment being erased when the material exceeds the glass transition temperature.

Figure 5.4 contains the normalized electrical resistance change during the first high temperature segment. The thermal cycling profile begins with a 30 min isothermal segment, followed by a ramp up to $150\text{ }^{\circ}\text{C}$ and 30 min of isotherm. The electrical resistance during this step initially increased and then decreased after about $100\text{ }^{\circ}\text{C}$. This was attributed to stress relaxation of the specimen as the material exceeded its glass transition temperature (T_g). The following $25\text{ }^{\circ}\text{C}$ resistance value was significantly reduced from that of the specimens just prior to the initial tensioning. It was not expected that this resistance value would be lower than the initial, although, given the tension condition present, Poisson's contraction in the transverse and through thickness directions could have had an effect.

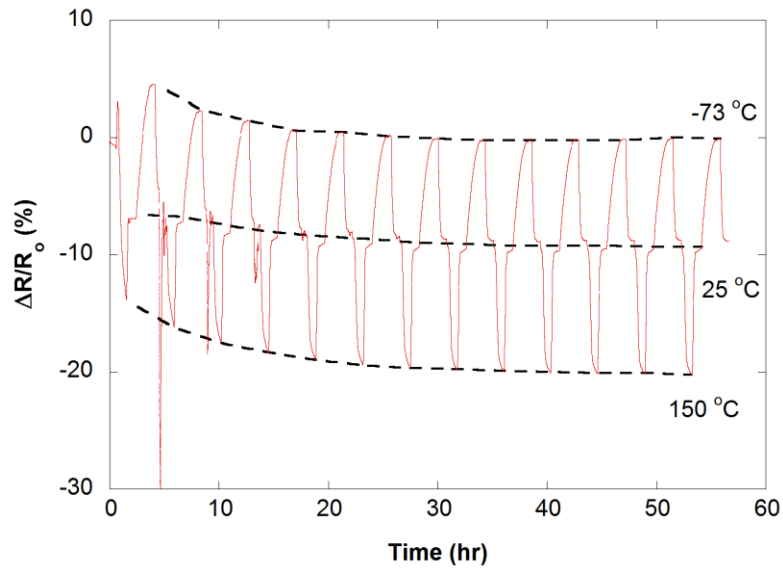


Figure 5.3: Typical electrical resistance trend during prolonged thermal cycling in an environmental chamber while constrained in a weathering fixture; dashed lines show maximum and minimum temperature contours and average 25°C contour.

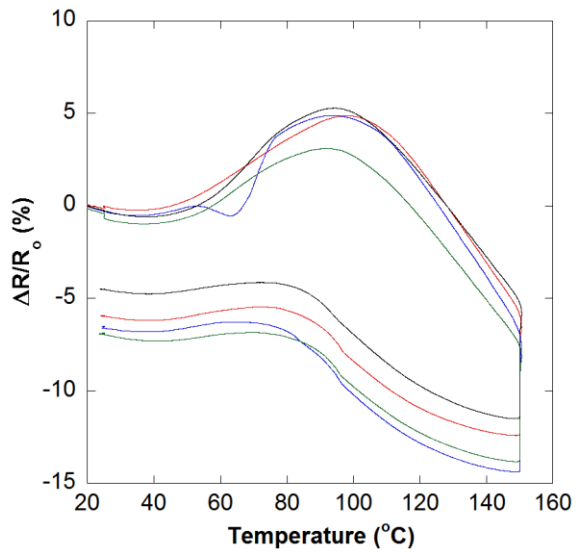


Figure 5.4: Normalized electrical resistance change during the initial thermal cycling segments showing permanent reduction in resistance due to stress relaxation above T_g .

The first cooling ramp to $-73\text{ }^{\circ}\text{C}$ (left, Figure 5.5) shows a trend very similar to the typical quasi static tensile results discussed previously. As temperature decreases from 25 to $-73\text{ }^{\circ}\text{C}$, the curves of the four specimens match very closely, but begin to diverge starting at $-10\text{ }^{\circ}\text{C}$ with the accumulation of damage. Here again, damage was evidenced by steps in the electrical resistance data. It is interesting to note that the specimens which showed initial damage in the pre-tensioning step, showed less damage during the first cooling ramp to $-73\text{ }^{\circ}\text{C}$. This should be expected because damage events do not repeat themselves, in general. In a previous work, during cyclic tensile loading of cross-ply glass fiber/CNT/epoxy composites, crack closure and reopening was observed during the unloading / reloading step where CNT-CNT junctions would come back into contact before separating again [59]. This resulted in a steep initial resistance / strain response and not the step-like behavior attributed to new crack formation. In this study the specimens remained under a tensile condition and this crack closure / reopening phenomenon was not observed. The normalized resistance change during the second cooling ramp showed little to no additional damage (right, Figure 5.5). With the exception of one specimen, these curves closely overlay each other. The results for the subsequent low temperature segments were much the same.

Edge replication was done before and after the tensioning segment, and again before removing the specimens from the weathering fixture. The images in Figure 5.6 show that some minor crack formation appeared in the 90° plies during the tensioning phase and that existing cracks were enlarged and new cracks were formed during the thermal cycling phase. Most of the additional damage was formed during the first

cooling ramp to $-73\text{ }^{\circ}\text{C}$ as evidenced by the step-like data trends in the left plot of Figure 5.5.

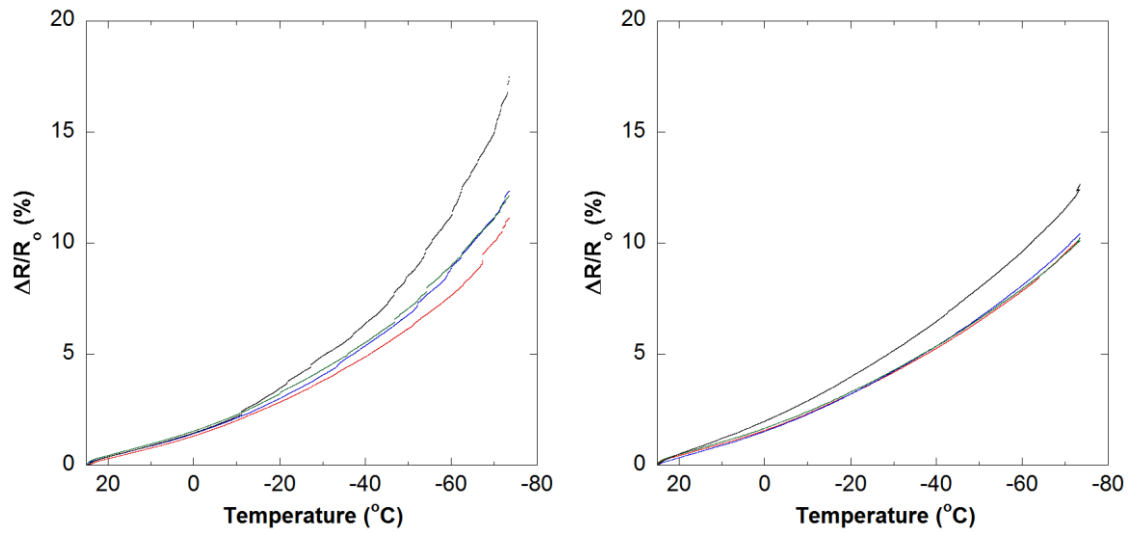


Figure 5.5: Normalized resistance change during the first two cooling ramps to $-73\text{ }^{\circ}\text{C}$; left: first cooling ramp showing step-like damage events, right: second cooling ramp showing little to no additional damage.

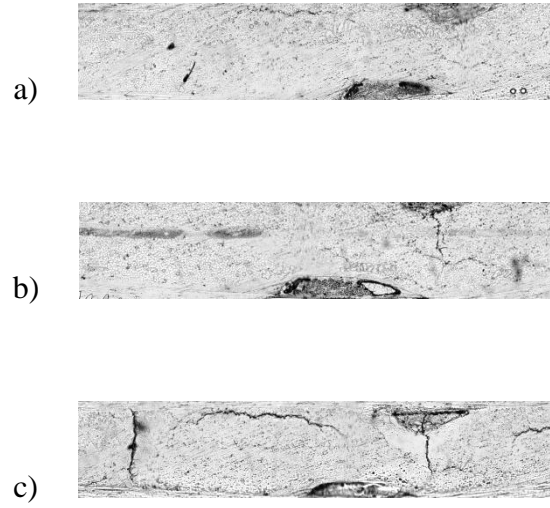


Figure 5.6: Micrographs of edge replicas showing crack growth and accumulation in 90 ° plies at different stages of testing; a) initial condition, b) pre-tensioned condition, and c) post-thermal cycled condition.

Given the transient phenomena observed during the thermal cycling tests (Figure 5.3), the data from the final thermal cycle were isolated for further analysis. The normalized electrical resistance curves for the four specimens are shown in Figure 5.7. The trends appear to have a negative temperature coefficient of resistance, whereas thermoresistive analysis results in Chapter 4 indicate that the 0.75 wt% CNT/VE material has an overall positive TCR. To explain this contradiction, it is convenient to recall the definition of mechanical strains $\{\varepsilon^M\}$ from classical lamination theory [60]:

$$\begin{Bmatrix} \varepsilon_x^M \\ \varepsilon_y^M \\ \gamma_{xy}^M \end{Bmatrix} = \begin{Bmatrix} \varepsilon_x^0 & zk_x \\ \varepsilon_y^0 & zk_y \\ \gamma_{xy}^0 & zk_{xy} \end{Bmatrix} - \begin{Bmatrix} \varepsilon_x^T \\ \varepsilon_y^T \\ \gamma_{xy}^T \end{Bmatrix} \quad (5.1)$$

where

$$\begin{Bmatrix} \varepsilon_x^T \\ \varepsilon_y^T \\ \gamma_{xy}^T \end{Bmatrix} = \Delta T \begin{Bmatrix} \alpha_x \\ \alpha_y \\ \alpha_{xy} \end{Bmatrix} \quad (5.2)$$

Because the laminate is symmetric and orthotropic, the plate curvatures k_{ij} are assumed to vanish and the thermal strains $\{\varepsilon^T\}$ are given by

$$\begin{Bmatrix} \varepsilon_x^T \\ \varepsilon_y^T \\ \gamma_{xy}^T \end{Bmatrix} = \Delta T \begin{Bmatrix} \alpha_T - \alpha_L \\ \alpha_L - \alpha_T \\ 0 \end{Bmatrix}. \quad (5.3)$$

Here, α_T and α_L are the coefficients of thermal expansion in the transverse and longitudinal lamina directions, respectively. A similar argument holds for the matrix and fiber constraints under thermal expansion; because VE has a much larger CTE than the glass fiber, when temperature is increased, the matrix is put into compression. This would explain the apparent negative TCR. The trends in Figure 5.7 indicate that electrical resistance goes like the y-direction mechanical strains, in which the slope change is caused the large increase in α_T , originating from the matrix thermal expansion change across T_g . It is also likely that the shape of this curve is influenced by changes in the polymer electrical properties as discussed in Section 4.2.

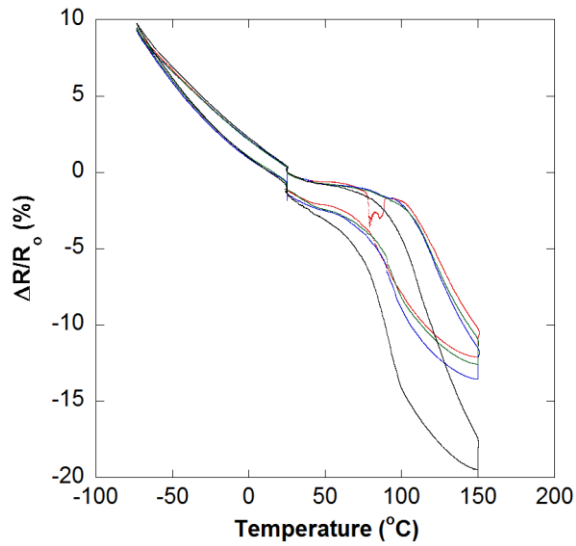


Figure 5.7: Normalized electrical resistance change during the final thermal cycle; slope change around 100 °C attributed to increase in matrix CTE across the glass transition.

5.1.3 Summary

A simple *in situ* sensing technique was used to monitor the progression of damage and stresses of cross ply $[0/90]_s$ composites of glass fiber and CNT/VE during a combined mechanical and thermal loading regime. Specimens were pre-tensioned using a special weathering fixture and subjected to repeated thermal cycling from -73 to 150 °C. It was found that significant crack growth and formation occurred during the testing, especially during the first cooling ramp to -73 °C when the 90 ° plies were subject to high tensile stresses due the mismatch of CTE between the transverse and fiber directions of the composite lamina. This CTE mismatch was also responsible for an apparent negative TCR, although the CNT/VE matrix material was shown to have an overall positive TCR. The results show that the CNT based sensing technique may be utilized under extreme conditions and give useful information about the progression of damage and stress state in the material. Future work in this area will investigate the

behavior of unidirectional composites under thermal and combined thermal and mechanical loading conditions.

Chapter 6

IN SITU CURE MONITORING OF GLASS FIBER/CARBON NANOTUBE/VINYL ESTER COMPOSITES

6.1 Results and Discussion

Torsional braid analysis was performed on vinyl ester specimens with different concentrations of dispersed oxidized carbon nanotubes. As a demonstration of the glass fiber/CNT/VE composite's sensitivity to shear strains, and to help establish the validity of the experimental approach, a plot of the electrical resistance versus time of a cured 1 wt% CNT/VE TBA specimen is shown in Figure 6.1.

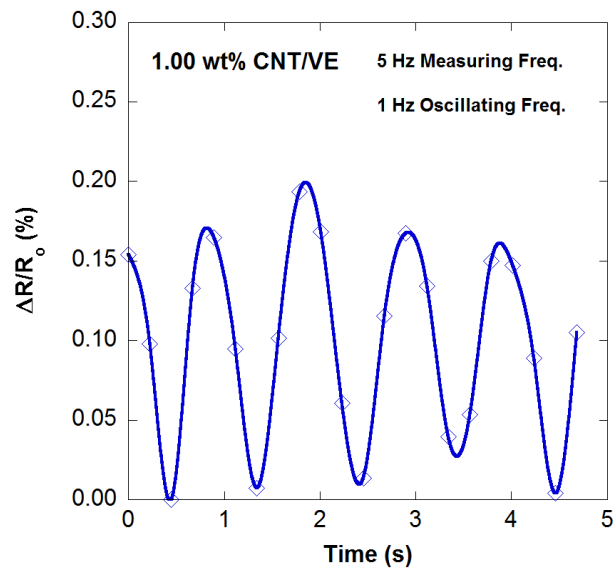


Figure 6.1: Electrical resistance response of a cured CNT/VE TBA specimen to a 1 Hz torsional oscillation; resistance versus time, data points traced with a cubic spline fit.

Plotted is the electrical resistance change of the specimen during a 1 Hz oscillating angular displacement showing strain sensitivity. The peaks in the resistance curve correspond to peaks in angular displacement applied by the rheometer.

6.1.1 Isothermal Cure of CNT/VE Composites

The isothermal cure profiles for TBA specimens are presented in Figure 6.2. Plotted are the storage and loss moduli (G' and G'' , respectively) and electrical resistances over the 2 hr 30 °C isothermal cure segment. For the Neat VE specimen, δ is plotted. Note that the TBA method does not measure the actual shear modulus G ; it is a relative measurement. The isothermal cure of VE and CNT/VE specimens progress from a liquid state, through gelation and vitrification [33]. The locations of these events can be determined from δ or the storage and loss moduli curves with time [61]. For the neat VE and CNT/VE specimens, gelation occurred at around 1000 s followed by vitrification. Comparison of the moduli curves suggest that the addition of CNTs may prolong the gelation time and increase the shear stiffness, and is the topic of an ongoing study.

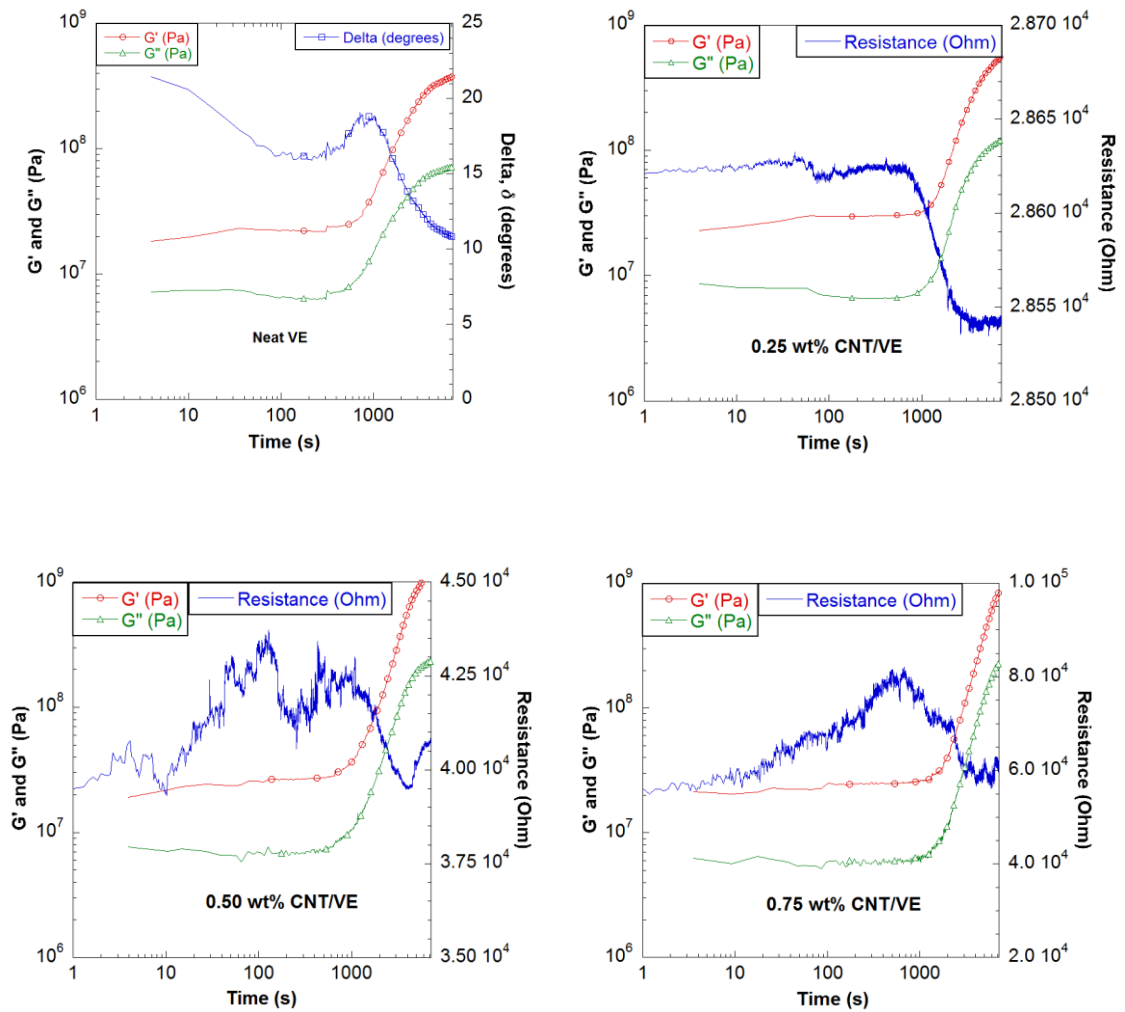


Figure 6.2: Comparison of isothermal cure data for neat VE and CNT/VE TBA specimens at 30 °C; storage and loss moduli and electrical resistance (delta for neat VE) versus time.

Of particular interest is the change in electrical resistance during isothermal cure. The electrical resistance tends for 0.25, 0.5 and 0.75 wt% CNT/VE specimens varied greatly. For the 0.75 wt% CNT specimen, the resistance increased until just

prior to gelation and then decreased. The 0.5 wt% CNT specimen increased and decreased in a similar fashion in the area of gelation, but continued to increase slightly during most of the remaining cure segment. The early portion, however, is quite erratic and noisy. The 0.25 wt% CNT specimen had the addition of conductive silver paint in the electrode area of the glass braid and the relative noise was greatly reduced, as well as the initial resistance value despite having a lower CNT concentration. This data is replotted in Figure 6.3 to clearly show the transitions occurring during cure and its correlation to the electrical resistance signal. At gelation the electrical resistance begins to decrease and the transition to the rubbery phase is marked by a leveling off of resistance. As the material continues to react, it hardens and forms a glassy state.

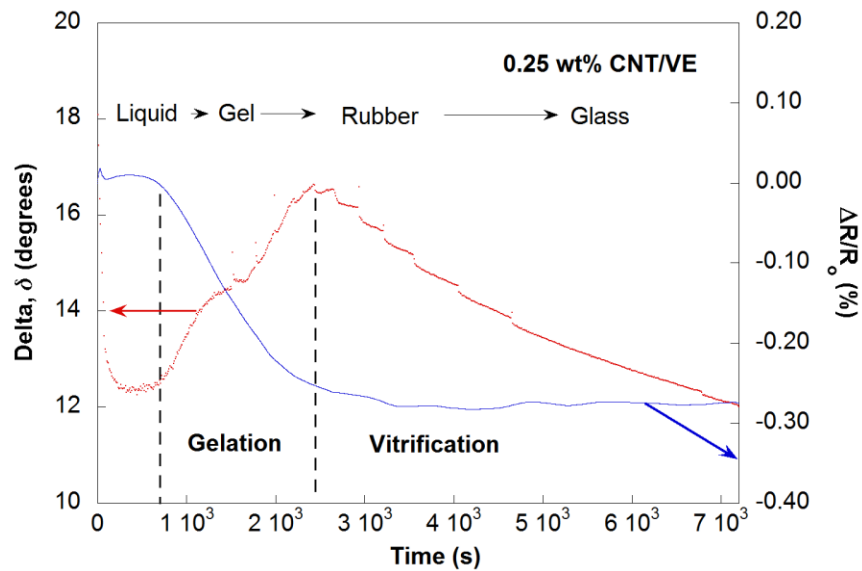


Figure 6.3: Delta and normalized electrical resistance change (filtered) for a 0.25 wt% CNT/VE specimen during isothermal cure at 30 °C; dashed lines separating gelation and vitrification regions.

6.1.2 Electrical Resistance during Continuous Heating Cure

The normalized electrical resistance change during continuous heating cure for 0.25 and 0.5 wt% CNT/VE specimens is shown in Figure 6.4. In these experiments, the temperature was continuously increased at 2 °C/min until 165 °C. The electrical resistance data show little change during gelation, but pronounced behavior during the remaining cure reaction. The left plot in Figure 6.4 describes the transformation processes taking place during continuous heating cure. The electrical resistance for the two specimens appears to follow the degree of cure; the reaction progresses rapidly during the first rubbery region, slows as the material become glassy, and then increases again after the glass transition temperature is exceeded, bring the material back into a rubbery state.

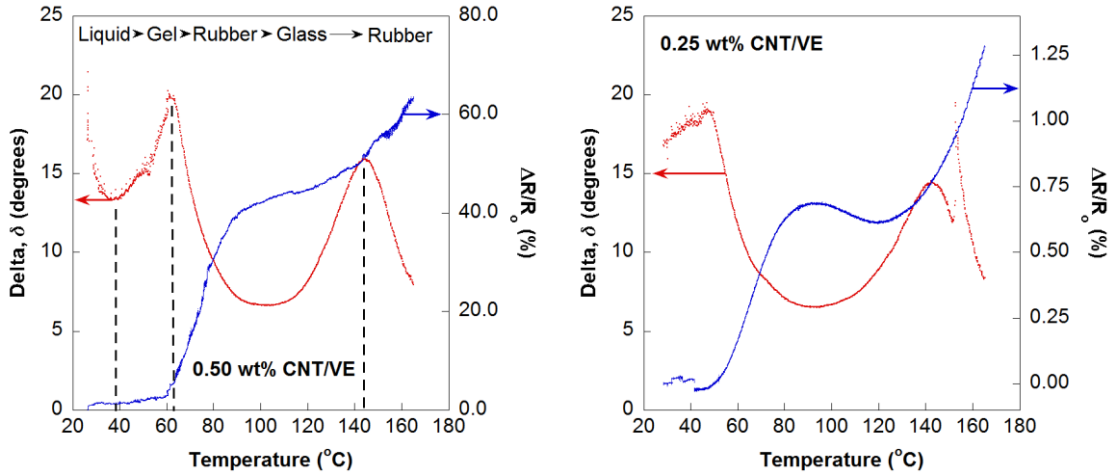


Figure 6.4: Electrical resistance change and delta during continuous heating cure for 0.5 and 0.25 wt% CNT specimens; left: dashed lines separating gelation and vitrification region and the glass transition. Note that the material passes back into the rubbery phase after the glass transition at 142 °C.

After continuous heating cure, the specimens were maintained at 165 °C for 2 hr to complete the reaction. The behavior shown in Figure 6.4 is also reflected in the post-cure step for the same specimens. The normalized electrical resistance change during this step is shown in Figure 6.5. Here, the trends show a diffusion-like increase in resistance similar to Figure 4.3. This was also observed during the post-cure of the isothermal cured specimens.

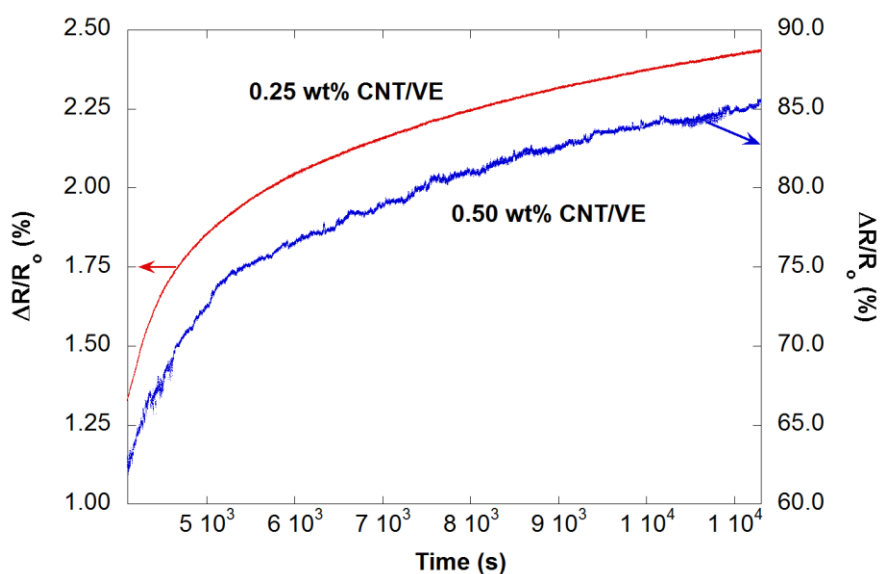


Figure 6.5: Electrical resistance change during post-cure of 0.25 and 0.5 wt% CNT/VE specimen after undergoing continuous heating cure; curves show diffusion-like increase in resistance.

6.1.3 Viscoelastic Trends during Torsional Braid Analysis

To compare the viscoelastic trends for specimens with isothermal cure versus continuous heating cure, the viscoelastic data for 0.5 wt% CNT/VE specimens are shown in Figure 6.6. The main difference between the two data sets are the shifts in T_g during the ramping segments. Since the cure reaction proceeds very quickly during

continuous heating cure, the initial T_g is 142 °C whereas the T_g after isothermal cure was 118 °C. This is because the reaction proceeds much faster during continuous heating cure due to the increase in temperature. In both cases, post-cure results in a further increase in T_g .

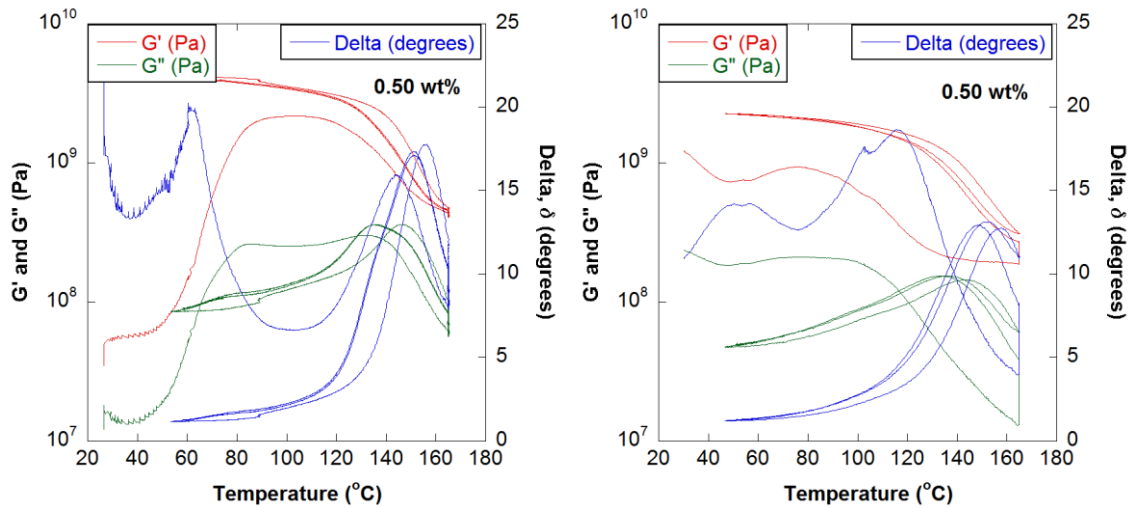


Figure 6.6: Comparison of viscoelastic trends during ramping segments of continuous heating cured, left (Profile III), and isothermal cured specimens of 0.5 wt% CNT/VE, right (Profile I).

The resistance and moduli data for the 0.25 and 0.5 wt% CNT/VE specimens are presented in Figure 6.7. In reference to Figure 3.5, the 0.25 and 0.5 wt% specimens were tested with temperature profiles II and I, respectively. The overall electrical resistance trends for the isothermal cure and post-cure segments were similar between the two specimens. Resistance generally decreased and then remained stable over the isothermal cure segment followed by a large increase during the ramp to, and

including, the post-cure segment. During the thermal cycling segments, in general, the specimens exhibited a positive temperature coefficient of resistance. Note that the sensitivity, or fractional change in resistance, of the 0.5 wt% CNT specimen is greater than the 0.25 wt% CNT specimen, about 112 % versus 4 % resistance change overall. The overall trends are in agreement with the observations made from Figures 6.4-5 and from the thermoresistive characterization work where electrical resistance was strongly influence by the progression of cure.

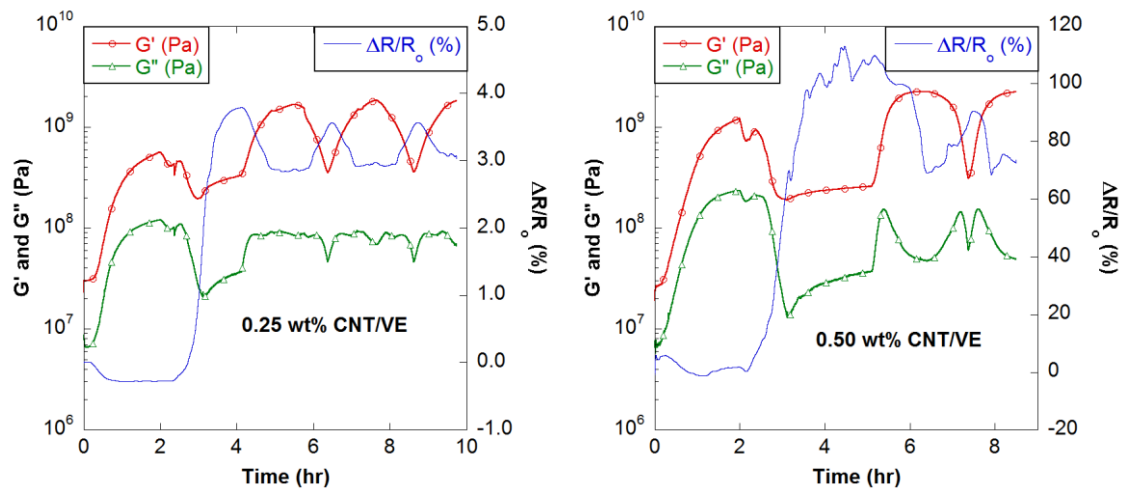


Figure 6.7: Electrical resistance change (filtered) and shear moduli during TBA tests; 0.25 and 0.5 wt% CNT/VE specimens using Profiles II and I, respectively (refer to Figure 3.5).

6.1.4 Summary

It was demonstrated that TBA type experiments could be conducted using a rheometer with torsion accessory and that *in situ* electrical resistance measurements could be taken without significantly reducing the quality of the viscoelastic measurement. Varying concentrations of dispersed CNTs showed different electrical

responses to isothermal cure and thermal cycling segments and electrical contacts were improved with the addition of conductive silver paint. The changes in electrical resistance were well correlated to the progression of cure during isothermal and continuous heating cure profiles. The electrical resistance data suggest that the *in situ* monitoring of cure processes may be achieved using a conducting network of CNTs dispersed in the polymer. This could have benefits for the composites industry in terms of quality, safety and reliability. In addition, the presence of the conducting CNT network in the final product would also allow for the built-in sensing capability during the lifetime of the product.

Chapter 7

CONCLUSIONS

Overall, the carbon nanotube-based sensing techniques developed in this work were highly sensitive to the changes occurring in the bulk material due to the effect of tunneling resistance. The same basic sensing approach may be used during the entire life cycle of composite parts, from the manufacturing processes and into the actual service environments, and to provide useful information about the state and health of the composite. This concept is presented in Figure 7.1.

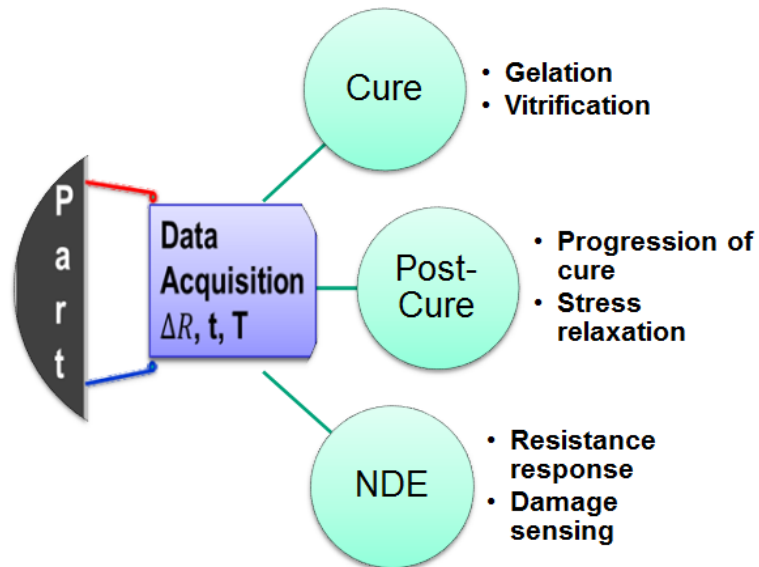


Figure 7.1: Schematic showing the sensing of cure, post-cure and service life using the carbon nanotube-based sensing technology developed in this work.

In the thermoresistive analysis of CNT/VE composites, specimens with 0.5 to 1 wt% CNT showed sensitivity to changes in the polymer interphase electrical properties. The 0.1 wt% CNT had a negative but near-zero TCR. It was found that with CNT content well above the percolation threshold, the sensitivity of the thermoresistive analysis technique in detecting changes in the polymer increased and that this sensitivity was comparable to the TSDC method. A transient increase in resistance at the high temperature set-point was attributed to further cure beyond that which is measurable by the DSC method.

During the combined mechanical and thermal loading conditions, it was found that significant crack growth and formation occurred in cross ply [0/90]_s composites of glass fiber and CNT/VE. This damage was observed in the 90 ° plies during the first cooling ramp to -73 °C as was evidenced in real-time by electrical resistance measurements and confirmed by edge replication. The mismatch in CTE between the matrix and fiber and between the longitudinal and transverse lamina directions was responsible for an apparent negative TCR, whereas the 0.75 wt% CNT/VE matrix material has a positive TCR. The results show that the CNT-based sensing technique may be utilized under extreme conditions and give useful information about the progression of damage and stress state in the material.

Torsional braid analysis was conducted using a rheometer with torsion accessory and electrical resistance measurements were taken *in situ* without reducing the quality of the viscoelastic measurement. Electrical resistance was found to be well correlated to the different stages of cure. The results data indicate that *in situ* monitoring of cure processes may be achieved during the manufacture of composite materials using a conducting network of CNTs dispersed in the polymer. This could

have positive benefits for the composites industry in terms of quality, safety and reliability. The presence of the conducting CNT network in the final product would also allow for the built-in sensing capability during the lifetime of the product.

It is recommended that future work be done on characterizing the thermoresistive response of fiber-reinforced multifunctional composites so that the response can be better understood and accurately predicted. In addition, the sensing of cure using carbon nanotubes should be demonstrated during full-scale manufacturing of composite panels. The methods developed in this work should be used to characterize multifunctional composites of epoxy and carbon nanotubes in order to compare the sensing performance and to further validate the experimental approaches.

REFERENCES

1. J Mijovic, K Lin. The effect of hygrothermal fatigue on physical mechanical-properties and morphology of neat epoxy-resin and graphite epoxy composite, *J Appl Polym Sci.* 30 (1985) 2527-2549.
2. TS Gates, MA Grayson, On the use of accelerated aging methods for screening high temperature polymeric composite materials, *AIAA.* 99-1296 (1998) 925-935.
3. B Abdel-Magid, S Ziaee, K Gass, M Schneider. The combined effects of load, moisture and temperature on the properties of E-glass/epoxy composites, *Compos.Struct.* 71 (2005) 320-326.
4. BD Argawal, LJ Broutman, K Chandrashekhara, *Environmental-Interaction Effects, Analysis and Performance of Fiber Composites*, 3rd ed., John Wiley & Sons, Inc, Hoboken, New Jersey, 2006, pp. 416-429.
5. FAA, 2012 National Aviation Research Plan, 2012 NARP. (2012) 51-57.
6. X Huang, J Gillespie, T Bogetti. Process induced stress for woven fabric thick section composite structures, *Compos.Struct.* 49 (2000) 303-312.
7. E Thostenson, Z Ren, T Chou. Advances in the science and technology of carbon nanotubes and their composites: a review, *Composites Sci.Technol.* 61 (2001) 1899-1912.
8. Y Ando, S Iijima. Preparation of carbon nanotubes by arc-discharge evaporation, *Jpn.J.Appl.Phys.Part 2 - Lett.* 32 (1993) L107-L109.
9. E Munoz, A Benito, L Estepa, J Fernandez, Y Maniette, M Martinez, et al. Structures of soot generated by laser induced pyrolysis of metal-graphite composite targets, *Carbon.* 36 (1998) 525-528.
10. P Collins, P Avouris. Multishell conduction in multiwalled carbon nanotubes, *Appl.Phys.A-Mater.Sci.Process.* 74 (2002) 329-332.
11. P Kim, L Shi, A Majumdar, P McEuen. Thermal transport measurements of individual multiwalled nanotubes, *Phys.Rev.Lett.* 87 (2001) 215502.
12. T Ebbesen, H Lezec, H Hiura, J Bennett, H Ghaemi, T Thio. Electrical conductivity of individual carbon nanotubes, *Nature.* 382 (1996) 54-56.

13. P Collins, M Arnold, P Avouris. Engineering carbon nanotubes and nanotube circuits using electrical breakdown, *Science*. 292 (2001) 706-709.
14. H Chen, B Wei, D Ma. Energy storage and management system with carbon nanotube supercapacitor and multidirectional power delivery capability for autonomous wireless sensor nodes, *IEEE Trans. Power Electron*. 25 (2010) 2897-2909.
15. X Li, J Rong, B Wei. Electrochemical behavior of single-walled carbon nanotube supercapacitors under compressive stress, *ACS Nano*. 4 (2010) 6039-6049.
16. E Thostenson, T Chou. On the elastic properties of carbon nanotube-based composites: modelling and characterization, *J. Phys. D- Appl. Phys.* 36 (2003) 573-582.
17. D Qian, E Dickey, R Andrews, T Rantell. Load transfer and deformation mechanisms in carbon nanotube-polystyrene composites, *Appl. Phys. Lett.* 76 (2000) 2868-2870.
18. FH Gojny, MHG Wichmann, B Fiedler, K Schulte. Influence of different carbon nanotubes on the mechanical properties of epoxy matrix composites – A comparative study, *Composites Sci. Technol.* 65 (2005) 2300-2313.
19. E Thostenson, W Li, D Wang, Z Ren, T Chou. Carbon nanotube/carbon fiber hybrid multiscale composites, *J. Appl. Phys.* 91 (2002) 6034-6037.
20. EJ Garcia, BL Wardle, A John Hart, N Yamamoto. Fabrication and multifunctional properties of a hybrid laminate with aligned carbon nanotubes grown *in situ*, *Composites Sci. Technol.* 68 (2008) 2034-2041.
21. H Qian, ES Greenhalgh, MSP Shaffer, A Bismarck. Carbon nanotube-based hierarchical composites: A review, *J. Mater. Chem.* 20 (2010) 4751-4762.
22. E Bekyarova, ET Thostenson, A Yu, H Kim, J Gao, J Tang, et al. Multiscale carbon nanotube-carbon fiber reinforcement for advanced epoxy composites, *Langmuir*. 23 (2007) 3970-3974.
23. C Li, ET Thostenson, T Chou. Sensors and actuators based on carbon nanotubes and their composites: A review, *Composites Sci. Technol.* 68 (2008) 1227-1249.

24. ET Thostenson, T Chou. Carbon nanotube networks: Sensing of distributed strain and damage for life prediction and self healing, *Adv Mater.* 18 (2006) 2837-2841.
25. L Gao, ET Thostenson, Z Zhang, T Chou. Coupled carbon nanotube network and acoustic emission monitoring for sensing of damage development in composites, *Carbon.* 47 (2009) 1381-1388.
26. L Gao, ET Thostenson, Z Zhang, J Byun, T Chou. Damage monitoring in fiber-reinforced composites under fatigue loading using carbon nanotube networks, *Philos.Mag.* 90 (2010) 4085-4099.
27. SM Friedrich, AS Wu, ET Thostenson, T Chou. Damage mode characterization of mechanically fastened composite joints using carbon nanotube networks, *Compos.Pt.A-Appl.Sci.Manuf.* 42 (2011) 2003-2009.
28. AS Lim, ZR Melrose, ET Thostenson, T Chou. Damage sensing of adhesively-bonded hybrid composite/steel joints using carbon nanotubes, *Composites Sci.Technol.* 71 (2011) 1183-1189.
29. L Gao, T Chou, ET Thostenson, Z Zhang, M Coulaud. In situ sensing of impact damage in epoxy/glass fiber composites using percolating carbon nanotube networks, *Carbon.* 49 (2011) 3382-3385.
30. C Li, ET Thostenson, T Chou. Dominant role of tunneling resistance in the electrical conductivity of carbon nanotube-based composites RID C-8998-2011 RID B-8587-2008, *Appl.Phys.Lett.* 91 (2007) 223114.
31. ET Thostenson, S Ziaee, T Chou. Processing and electrical properties of carbon nanotube/vinyl ester nanocomposites, *Composites Sci.Technol.* 69 (2009) 801-804.
32. Q An, AN Rider, ET Thostenson. Electrophoretic deposition of carbon nanotubes onto carbon-fiber fabric for production of carbon/epoxy composites with improved mechanical properties, *Carbon* (2012).
33. S Ziaee, G Palmese. Effects of temperature on cure kinetics and mechanical properties of vinyl-ester resins, *J.Polym.Sci.Pt.B-Polym.Phys.* 37 (1999) 725-744.
34. F Gojny, M Wichmann, B Fiedler, I Kinloch, W Bauhofer, A Windle, et al. Evaluation and identification of electrical and thermal conduction mechanisms in carbon nanotube/epoxy composites, *Polymer.* 47 (2006) 2036-2045.

35. E Kymakis, G Amaratunga. Electrical properties of single-wall carbon nanotube-polymer composite films, *J.Appl.Phys.* 99 (2006) 084302.
36. Y Simsek, L Ozyuzer, AT Seyhan, M Tanoglu, K Schulte. Temperature dependence of electrical conductivity in double-wall and multi-wall carbon nanotube/polyester nanocomposites, *J.Mater.Sci.* 42 (2007) 9689-9695.
37. P Cardoso, J Silva, D Klosterman, JA Covas, FWJ van Hattum, R Simoes, et al. The role of disorder on the AC and DC electrical conductivity of vapour grown carbon nanofibre/epoxy composites, *Composites Sci.Technol.* 72 (2012) 243-247.
38. M Mohiuddin, SV Hoa. Temperature dependent electrical conductivity of CNT-PEEK composites, *Composites Sci.Technol.* 72 (2011) 21-27.
39. M Mohiuddin, S Van Hoa. Electrical resistance of CNT-PEEK composites under compression at different temperatures, *Nanoscale Res.Lett.* 6 (2011) 419.
40. M Mu, AM Walker, JM Torkelson, KI Winey. Cellular structures of carbon nanotubes in a polymer matrix improve properties relative to composites with dispersed nanotubes, *Polymer.* 49 (2008) 1332-1337.
41. A Das, KW Stoeckelhuber, R Jurk, M Saphiannikova, J Fritzsche, H Lorenz, et al. Modified and unmodified multiwalled carbon nanotubes in high performance solution-styrene-butadiene and butadiene rubber blends, *Polymer.* 49 (2008) 5276-5283.
42. G Hu, C Zhao, S Zhang, M Yang, Z Wang. Low percolation thresholds of electrical conductivity and rheology in poly(ethylene terephthalate) through the networks of multi-walled carbon nanotubes, *Polymer.* 47 (2006) 480-488.
43. J Sandler, J Kirk, I Kinloch, M Shaffer, A Windle. Ultra-low electrical percolation threshold in carbon-nanotube-epoxy composites, *Polymer.* 44 (2003) 5893-5899.
44. ASTM D257-99. Standard test methods for DC resistance or conductance of insulating materials, ASTM International (2005).
45. P Avouris. Carbon nanotube electronics, *Chem.Phys.* 281 (2002) 429-445.

46. TS Gates, KS Whitley, RW Grenoble, T Bandorawalla. Thermal/mechanical durability of polymer-matrix composites in cryogenic environments, AIAA-2003-7408. (2003).
47. K Whitley, T Gates. Thermal/mechanical response of a polymer matrix composite at cryogenic temperatures, AIAA J. 42 (2004) 1991-2001.
48. W Zukas. Torsional braid analysis of the aromatic amine cure of epoxy-resins, J Appl Polym Sci. 53 (1994) 429-440.
49. J Lee, J Hwang, J Gillham. Erasure below glass-transition temperature of effect of isothermal physical aging in fully cured epoxy/amine thermosetting system, J Appl Polym Sci. 81 (2001) 396-404.
50. M Stone, B Fink, T Bogetti, J Gillespie. Thermo-chemical response of vinyl-ester resin, Polym.Eng.Sci. 40 (2000) 2489-2497.
51. J Gillham. The TBA torsion pendulum: a technique for characterizing the cure and properties of thermosetting systems, Polym.Int. 44 (1997) 262-276.
52. W Lu, T Chou, ET Thostenson. A three-dimensional model of electrical percolation thresholds in carbon nanotube-based composites, Appl.Phys.Lett. 96 (2010) 223114-223114-3.
53. G Kampf, Thermoanalytic Methods, Characterization of Plastics by Physical Methods: Experimental Techniques and Practical Application, Hanser Publishers, New York, 1986, pp. 197-207.
54. H St-Onge. Electrical conduction in 3-percent carbon-filled polyethylene - part 1: low-field results, IEEE Transactions on Electrical Insulation. E1-11 (1976) 20-27.
55. MS Gaur, BS Rathore, PK Singh, A Indolia, AM Awasthi, S Bhardwaj. Thermally stimulated current and differential scanning calorimetry spectroscopy for the study of polymer nanocomposites, J.Therm.Anal.Calorim. 101 (2010) 315-321.
56. G Kampf, Electrical Methods, Characterization of Plastics by Physical Methods: Experimental Techniques and Practical Application, Hanser Publishers, New York, 1986, pp. 197-207.

57. T Goel, A Tripathi, B Rao, M Choudhary, V Choudhary, I Varma. Vinyl ester resins. II. Effect of styrene on electrical-properties, *J Appl Polym Sci.* 30 (1985) 1491-1497.
58. L Gao, T Chou, ET Thostenson, Z Zhang. A comparative study of damage sensing in fiber composites using uniformly and non-uniformly dispersed carbon nanotubes, *Carbon.* 48 (2010) 3788-3794.
59. L Gao, ET Thostenson, Z Zhang, T Chou. Sensing of damage mechanisms in fiber-reinforced composites under cyclic loading using carbon nanotubes, *Adv.Funct.Mater.* 19 (2009) 123-130.
60. BD Argawal, LJ Broutman, K Chandrashekhara, *Hygrothermal Stresses in Laminates, Analysis and Performance of Fiber Composites*, 3rd ed., John Wiley & Sons, Inc, Hoboken, New Jersey, 2006, pp. 263-272.
61. S Simon, J Gillham. Thermosetting cure diagrams - calculation and application, *J Appl Polym Sci.* 53 (1994) 709-727.

Appendix A

REFERENCES FOR REPRODUCED FIGURES

- Figure 1.2. E Thostenson, T Chou. On the elastic properties of carbon nanotube-based composites: modelling and characterization, *J.Phys.D-Appl.Phys.* 36 (2003) 573-582.
- Figure 1.3. D Qian, E Dickey, R Andrews, T Rantell. Load transfer and deformation mechanisms in carbon nanotube-polystyrene composites, *Appl.Phys.Lett.* 76 (2000) 2868-2870.
- Figure 1.4.a. EJ Garcia, BL Wardle, A John Hart, N Yamamoto. Fabrication and multifunctional properties of a hybrid laminate with aligned carbon nanotubes grown *in situ*, *Composites Sci.Technol.* 68 (2008) 2034-2041.
- Figure 1.4.b. E Bekyarova, ET Thostenson, A Yu, H Kim, J Gao, J Tang, et al. Multiscale carbon nanotube-carbon fiber reinforcement for advanced epoxy composites, *Langmuir.* 23 (2007) 3970-3974.
- Figure 1.5. C Li, ET Thostenson, T Chou. Sensors and actuators based on carbon nanotubes and their composites: A review, *Composites Sci.Technol.* 68 (2008) 1227-1249.
- Figure 1.6. L Gao, ET Thostenson, Z Zhang, T Chou. Coupled carbon nanotube network and acoustic emission monitoring for sensing of damage development in composites, *Carbon.* 47 (2009) 1381-1388.
- Figure 2.1-2. ET Thostenson, S Ziaee, T Chou. Processing and electrical properties of carbon nanotube/vinyl ester nanocomposites, *Composites Sci.Technol.* 69 (2009) 801-804.
- Figure 2.3. Q An, AN Rider, ET Thostenson. Electrophoretic deposition of carbon nanotubes onto carbon-fiber fabric for production of carbon/epoxy composites with improved mechanical properties, *Carbon* (2012).
- Figure 2.4. E Bekyarova, ET Thostenson, A Yu, H Kim, J Gao, J Tang, et al. Multiscale carbon nanotube-carbon fiber reinforcement for advanced epoxy composites, *Langmuir.* 23 (2007) 3970-3974.

Appendix B

AUTHOR'S PUBLICATIONS AND WORKS IN PROGRESS

1. K Lasater, ET Thostenson. Thermoresistive characterization of composite materials, Vishay Precision Foil Case Study (2012).
2. K Lasater, ET Thostenson, WR Yu. *In situ* monitoring of cure and viscoelastic behavior of composites using carbon nanotubes, SAMPE 2012, Baltimore, MD, May 21-24 (2012).
3. K Lasater, ET Thostenson. *In situ* thermoresistive characterization of multifunctional composites of carbon nanotubes, Submitted (2012).
4. K Lasater, ET Thostenson. Carbon nanotube-based *in situ* sensing for total health monitoring: cure, post-cure, and service of composite materials, In progress.

Appendix C

BIOGRAPHY

The author graduated from Winona State University with a Bachelor of Science in Composite Materials Engineering, *Magna cum Laude* in 2010. His interest in composite materials grew during his experience working as a mechanic at a local bicycle shop throughout his high school and undergraduate career. During that time, he witnessed leaps and bounds in bicycle technology and the general acceptance of composite materials as the material of choice for high-end bicycle structures because of its lightness of weight and tailorable properties and ride characteristics. In collaboration with his boss and customers, he designed and tested a prototype bicycle hub with an original “internal flange” design which utilized a composite shell as its primary structure.

During his graduate career, the author was awarded a National Science Foundation Fellowship to conduct research at Seoul National University (SNU) and the Korea Institute of Materials Science (KIMS) in the Republic of Korea. During this time, the author served as Principal Investigator and collaborated with his host, Professor Woong-Ryeol Yu, on the project of cure monitoring using dispersed carbon nanotubes in vinyl ester resin. The author attended the ICCM 18 conference on Jeju Island, Korea at the end of the eight week research program at SNU and KIMS. The results of the cure monitoring study were presented at SAMPE 2012 in Baltimore, MD. The author will begin a career as a mechanical engineer in the aerospace industry following graduation.